M 2023

U.PORTO
FEUP FACULDADE DE ENGENHARIA
UNIVERSIDADE DO PORTO

PURIFICATION OF GREEN FUELS BY INNOVATIVE MEMBRANE SEPARATION PROCESSES

LAURA ALVES PEREIRA

MASTER THESIS IN CHEMICAL ENGINEERING
PRESENTED TO THE FACULTY OF ENGINEERING
OF THE UNIVERSITY OF PORTO

Master in Chemical Engineering

Purification of green fuels by innovative membrane separation processes

Master dissertation

of

Laura Alves Pereira

Developed within the course of dissertation

held in

Companies





Supervisor at FEUP: **Dr. Carlos Gabriel Bernardo**

Joint supervisor at FEUP: **Prof. Adélio Mendes**

Coordinator at Capwatt: **Eng. Joana Vasconcelos**

Coordinator at Carbopora: **Manuel Lopes**





July 2023

Acknowledgment

A lot of people contributed to the success of this work, either directly or indirectly, that deserve a thank you.

Firstly, I want to thank my supervisor at FEUP, Dr. Gabriel Bernardo, for being always available and for providing valuable suggestions to ensure that I would present the best work possible. I also want to thank Prof. Adélio Mendes for the help and knowledge shared during these last few months.

To Capwatt colleagues that I had the pleasure of interacting with and always made me feel welcome and included. In particular to my coordinator at Capwatt, Eng. Joana Vasconcelos, I would like to thank for the genuine interest in my work and for all the advice and motivation during this period. To Telmo for the suggestions and critical thinking and all the team of Carbopora, for the opportunity of doing this work in a company specialized in the field.

A special thank you to Tiago Araújo for his dedication from the first minute. Thank you for all the knowledge, the patience, for the emails at 1 am and for the waiting time while staring at a screen searching for peaks. The last few months had been incredibly challenging, and Tiago never let me get demotivated. I am very grateful to have worked with him.

I would like to thank my colleagues at LEPABE for integrating me and for being available every time I needed. A special thank you to Francisco, Paranjeet, Cátia and Tiago Santos for generously dedicating their time to help and teach me.

Thank you to Luciana Rocha and Luís Carlos for the SEM images and the Raman tests, respectively, and to the professionals who performed the other characterization tests.

To my friends for making this journey so much better, it wouldn't have been the same without them. Thank you for all the laughter and for holding back my tears and specially for supporting me no matter what, not only throughout this last semester but also the entire five years.

Finally, to my family, who may not have fully understood my work but always believed in me and made an effort to keep up and be interested in it. Thank you to Rita, who was always there for me and knew how to calm me down and how to motivate me when I most needed.

Professor Adélio Mendes and Dr Gabriel Bernardo, supervisors of this dissertation are integrated members of LEPABE – Laboratory for Process Engineering, Environment, Biotechnology and Energy, financially supported by LA/P/0045/2020 (ALiCE), UIDB/00511/2020 and UIDP/00511/2020 (LEPABE), funded by national funds through FCT/MCTES (PIDDAC).

Abstract

The urgent need to meet the goals set in the Paris Agreement requires the exploration of new technologies across all sectors. Regarding the transportation industry, while electrification and hydrogen are promising solutions for light duty transport, for maritime shipping and aviation it is necessary the use of liquid green fuels. Renewable methanol, derived from renewable sources, like biomass, green hydrogen and renewable CO_2, has a huge potential to replace fossil fuels. However, its production generates water as a by-product that needs to be removed. Currently, the purification of methanol is done through energy intensive distillation towers, increasing the cost of e-methanol compared with traditional fuels.

Membrane technology offers an environmentally friendly and energy efficient alternative for purifying green fuels. Among various types of membranes, carbon molecular sieve membranes, CMSMs, are one of the most promising type of membranes due to their turbostratic structure that combines a pore size distribution with micropores connecting ultramicropores, that are responsible for molecular sieving. Typically, the carbon membranes have low affinity to water molecules. However, in this project, non-supported hydrophilic cellulose-based carbon molecular sieve membranes, with boehmite nanoparticules were developed to effectively separate water from organic solvents, namely methanol and ethanol.

A series of carbon membranes with varying amounts of boehmite and subjected to different carbonization atmospheres were successfully produced. The characterization tests revealed that boehmite changes the microporous structure of the membranes and increases their affinity for water. These findings corroborate the results obtained in the single gas permeation tests, where the permeability and selectivity values increased, for all gases tested. The humidified gas permeation tests demonstrated the membranes' ability to permeate water molecules, with higher levels of boehmite content leading to increased permeability for humidified gas.

Finally, a proof of concept was carried out for the water/solvent separation tests. An installation was made where mixtures with methanol and ethanol were tested at two distinct temperatures. Analysis of the chromatograms revealed that water was present in the permeate stream. The highest value of permeance was obtained for the separation of water/methanol at 200 °C, of 0.502 $mol \cdot m^{-2} \cdot h^{-1} \cdot kPa^{-1}$. After the tests conducted at 200 °C, the membrane underwent a transformation, becoming hydrophobic and acquiring new components within its chemical structure.

Keywords: Green fuels, CMSM, boehmite, permeability, water/solvent separation.

Resumo

A necessidade urgente de cumprir os objetivos estabelecidos no Acordo de Paris exige a exploração de novas tecnologias em todos os sectores. No que diz respeito à indústria dos transportes, enquanto a eletrificação e o hidrogénio são soluções promissoras para os transportes ligeiros, para a navegação marítima e aviação é necessária a utilização de combustíveis líquidos renováveis. O metanol renovável, derivado de fontes renováveis como biomassa, hidrogénio e CO_2 verde, tem um enorme potencial para substituir os combustíveis fósseis. No entanto, a sua produção gera água como subproduto. Atualmente, a purificação do metanol é feita através de torres de destilação que consomem muita energia, aumentando o custo do e-metanol em comparação com os combustíveis tradicionais.

A tecnologia de membranas oferece uma alternativa ecológica e energeticamente eficiente para a purificação de combustíveis verdes. Entre os vários tipos de membranas, as membranas de peneira molecular de carbono, CMSM, são um dos tipos de membranas mais promissores devido à sua estrutura turbostática, que combina uma distribuição do tamanho dos poros com microporos e ultramicroporos, que são responsáveis pela peneiração molecular. Tipicamente, as membranas de carbono têm baixa afinidade a moléculas de água, no entanto, neste projeto foram desenvolvidas membranas hidrofílicas de peneira molecular de carbono não suportadas, à base de celulose com nanopartículas de boehmite, para separar eficazmente a água de solventes orgânicos, nomeadamente metanol e etanol.

Foram produzidas várias membranas de carbono com quantidades variáveis de boehmite e sujeitas a diferentes atmosferas de carbonização. Os testes de caraterização revelaram que a boehmite altera a estrutura microporosa das membranas e aumenta a sua afinidade pela água. Estas conclusões corroboram os resultados obtidos nos ensaios de permeação monocomponente, onde os valores de permeabilidade e seletividade aumentaram, para todos os gases testados. Os ensaios de permeação a gás humidificado demonstraram a capacidade das membranas para permear moléculas de água e que, mais uma vez, um teor de boehmite mais elevado conduziu a um aumento da permeabilidade para o gás humidificado.

Finalmente, foi efetuada uma prova de conceito para os ensaios de separação de água e solventes orgânicos. Foi construída uma instalação onde foram testadas misturas com metanol e etanol a duas temperaturas distintas. A análise dos cromatogramas revelou que água estava presente no permeado. O valor mais elevado de permeância foi obtido para a separação de água/metanol a 200 °C, de 0.502 $mol \cdot m^{-2} \cdot h^{-1} \cdot kPa^{-1}$. Após os testes realizados a 200 °C, a membrana sofreu uma transformação, tornando-se hidrofóbica e adquirindo novos componentes na sua estrutura química.

Palavras-chave: Combustíveis verdes, CMSM, boehmite, permeabilidade, separação água/solvente.

Declaration

I hereby declare, under word of honor, that this work is original and that all non-original contributions is indicated and due reference is given to the author and source

July 3rd,

Laura Alves Pereira

Index

1 Introduction 1

1.1 Framing and presentation of the work 1

1.2 Presentation of the companies 3

1.3 Contribution of the author to the work 4

1.4 Organization of the dissertation 4

2 Context and State of the art 5

2.1 Membranes 5

2.2 Carbon Molecular Sieve Membranes (CMSMs) 10

2.3 CMSMs for gas separation 12

2.4 Water/solvent separation with membrane technology 13

3 Materials and Methods 17

3.1 Materials 17

3.2 Preparation of cellulose precursor membranes 17

3.3 Preparation of cellulose based CMSMs 17

3.4 CMSM characterization 18

3.4.1 Scanning Electron Microscopy (SEM) and Energy Dispersive Spectroscopy (EDS) 18

3.4.2 Thermogravimetric Analysis (TGA) 19

3.4.3 Fourier Transform Infrared Spectroscopy with Attenuated Total Reflection (FTIR-ATR) .. 19

3.4.4 X-Ray Diffraction analysis (XRD) 19

3.4.5 Raman spectroscopy 19

3.4.6 Water contact angle measurements 20

3.5 Gas permeation test 20

3.6 Water/solvent separation tests 21

4 Results and Discussion 23

4.1 Characterization tests 23

4.1.1 Preparation of CMSM 23

4.1.2 Scanning Electron Microscopy (SEM) and Energy Dispersive Spectroscopy (EDS) 24

4.1.3 Thermogravimetric Analyses (TGA) 26
4.1.4 Fourier Transform Infrared Spectroscopy (FTIR) 27
4.1.5 X-Ray Diffraction analysis XRD 28
4.1.6 Raman spectroscopy 29
4.1.7 Water contact angle 30
4.2 Permeation tests 31
4.2.1 Boehmite content 31
4.2.2 Carbonization atmosphere 34
4.2.3 Humidified gas permeation experiments 35
4.3 Water/solvent separation tests 36
4.3.1 Gas chromatography and permeation results 36
4.3.2 Post experiments characterization tests 39
5 Conclusion 41
6 Assessment of the work done 43
6.1 Objectives Achieved 43
6.2 Other Work Carried Out 43
6.3 Limitations and Future Work 43
6.4 Final Assessment 44
7 References 45
Appendix A- Setup of the installation and results 51
A.1 Preparation of the CMSMs 51
A.2 Installations of the different separation tests 51
A.3 Deduction of the permeance of the CMSMs to water/solvent permeation tests . 53
A.4 Results 55

List of Figures

***Figure 1.1**. (**A**) CO2 emission by sector (reproduced from [3]); (**B**) Sustainable development scenario for transport emissions until 2070 (reproduced from [5]).* 1

***Figure 1.2**. Scheme of Capwatt's methanol production process.* 3

***Figure 2.1**. Scheme of membrane separation (reproduced from [22]).* 5

***Figure 2.2**. Membrane classification according to the pore size.* 6

***Figure 2.3**. (**A**) symmetric structure (reproduced from [2]); (**B**) asymmetric structure (reproduced from [24]).* 6

***Figure 2.4**. Transport mechanisms through a porous membrane: (**a**) Knudsen diffusion; (**b**) surface diffusion; (**c**) capillary condensation; (**d**) molecular sieving (reproduced from [36]).* 8

***Figure 2.5**. Robeson upper bound for O_2/N_2 separation (reproduced from [27]).* 9

***Figure 2.6**. Turbostratic structure of a CMSM (reproduced from [45]).* 10

***Figure 2.7**. Different geometries of CMSMs (reproduced from [42]).* 11

***Figure 3.1**. Experimental setup for water/solvent separation tests.* 22

***Figure 4.1**. Cellulose membrane with boehmite nanoparticles (**A**) before and (**B**) after carbonization.* 23

***Figure 4.2**. SEM images of the precursor film (**A1**) without boehmite and a boehmite content of (**B1**) 0.55 wt. %, (**C1**) 1.10 wt. %, (**D1**) 2.15 wt. % in normal plan (left) and cross section (right); SEM images of (**A2**) CMSM 0, (**B2**) CMSM 0.55, (**C2**) CMSM 1.10 and (**D2**) CMSM 2.15.* 25

***Figure 4.3**. SEM images of (**A**) CMSM CO_2, (**B**) CMSM N_2 and (**C**) CMSM N_2+H_2.* 25

***Figure 4.4**. TGA of the (**A**) polymeric precursor and (**B**) the carbon membranes.* 26

***Figure 4.5**. FTIR spectra of (**A**) the precursor films and (**B**) respective CMSMs.* 27

***Figure 4.6**. XRD analysis of the CMSMs produced with (**A**) different quantities of boehmite and (**B**) carbonized under different atmospheres.* 28

***Figure 4.7**. Raman spectra of the CMSMs produced with(**A**) different quantities of boehmite and (**B**) carbonized at different atmospheres.* 30

***Figure 4.8**. Water contact angle measurements of the CMSMs produced with (**A**) different quantities of boehmite and (**B**) carbonized under different atmospheres.* 31

***Figure 4.9**. (**A**) Single gas permeabilities and (**B**) ideal selectivities of the CMSMs produced with different quantities of boehmite.* 32

***Figure 4.10**. Robeson plots for the CMSMs produced with different quantities of boehmite for (**A**) H_2/N_2, (**B**) O_2/N_2, (**C**) H_2/CO_2 and (**D**) CO_2/N_2 separations.* 33

***Figure 4.11**. Permeability and selectivity in function of (**A**) the d-spacing and (**B**) A_D/A_G 33*

***Figure 4.12**. (**A**) Single gas permeabilities and (**B**) ideal selectivities of the CMSMs produced with different carbonization atmospheres. 34*

***Figure 4.13**. Robeson plots for the CMSMs produced with different carbonization atmospheres for (**A**) H_2/N_2, (**B**) O_2/N_2, (**C**) H_2/CO_2 and (**D**) CO_2/N_2 separations. 35*

***Figure 4.14**. Permeability and selectivity in function of the A_D/A_G. 35*

***Figure 4.15**. Chromatogram of the direct injections of methanol and ethanol. 37*

***Figure 4.16**. Chromatogram of the 50/50 vol. % methanol-water experiment at (**A**) 120 °C and (**B**) 200 °C. 38*

***Figure 4.17**. Chromatogram of the 70/30 vol. % ethanol-water experiment at 120 °C. 38*

***Figure 4.18**. SEM image for the CMSM 1.10 post experiment. 39*

***Figure 4.19**. FTIR spectra of CMSM 1.10 pre and post experiment and new bands assignments. 40*

***Figure 4.20**. (**A**) EDS spectrum and (**B**) water contact angle measurements for the CMSM 1.10 pre and post experiment 40*

***Figure 6.1**. Suggestion of future setup for water/solvent separation tests. 44*

***Figure A.1**. Carbonization steps to prepare the cellulose-based CMSMs. 51*

***Figure A.2**. Experimental setup for single gas permeation experiments (reproduced from [11]). 51*

***Figure A.3**. Photographs of the laboratory installation for single gas permeation tests; (**A**) feed to the membrane module and (**B**) permeate tank. 52*

***Figure A.4**. Initial installation for water/solvent separation tests. 52*

***Figure A.5**. (**A**) Photographs of the initial laboratory installation for water/solvent separation tests and a (**B**) close up of the membrane module inside the oven and (**C**) the cold trap with a vacuum pump. 52*

***Figure A.6**. Photographs of (**A**)the laboratory installation for water/solvent separation tests using the dew point meter; (**B**) close up of the humidity sensor; (**C**) close up of the feed and HPLC pump and (**D**) close up of the GC. 53*

***Figure A.7**. Flow behavior at the permeate side of the membrane (adapted from [67]) 53*

***Figure A.8**. TGA plot and correspondent derivate curve of the precursor correspondent to (**A**) CMSM 0; (**B**) CMSM 0.55; (**C**) CMSM 1.10 and (**D**) CMSM 2.15. ..... 55*

***Figure A.9**. CMSM surface of a sample (**A**)with and (**B**) without boehmite. 56*

***Figure A.10**. (**A**) Raman and (**B**) XRD spectra for the CMSM 1.10 pre and post experiment. 57*

List of Tables

Table 1. *Comparison of pervaporation membranes applied to aqueous ethanol dehydration.* *15*

Table 2. *Comparison of pervaporation membranes applied to aqueous methanol dehydration.* *16*

Table 3. *Preparation conditions of the different CMSMs.* *18*

Table 4. *Dimensions of the cellulose membrane before and after carbonization.*..... *24*

Table 5. *Mass percentage of the membrane composition given by EDS technique*..... *25*

Table 6. *Summary of the information obtained from TGA.* *27*

Table 7. *d-spacing values obtained with XRD analysis*..... *29*

Table 8. A_D/A_G *values obtained by Raman technique*..... *30*

Table 9. *Robeson index of the CMSMs produced with different quantities of boehmite.* *32*

Table 10. *Robeson index of the CMSMs produced with different carbonization atmospheres.* *34*

Table 11. *Humidified gas permeability of the CMSMs produced with different quantities of boehmite and different carbonization atmospheres.*..... *36*

Table 12. *Permeance results for the water/solvent separation experiments.* *39*

Notation and Glossary

a	Slope of log-log relationship	m^2
A_{cell}	Working area of the membrane cell	m^2
A_D	Area of the D peak	cm^2
A_G	Area of the G peak	cm^2
c	Concentration	$mg \cdot L^{-1}$
d	d-spacing	nm
dp	Pore diameter	nm
D	Diffusivity	$m^2 \cdot s^{-1}$
J	Flux	$g \cdot m^{-2} \cdot h^{-1}$
k	Front factor	barrer
m	Slope of Robeson upper bound	
l	Membrane thickness	μm
M	Molar mass	$g \cdot mol^{-1}$
n	Diffraction order	
p	Partial pressure	Pa
P	Permeability	barrer
P_{tot}	Total pressure in the permeate side	Pa
r	Membrane radius	mm
R	Gas constant	$Pa \cdot m^3 \cdot mol^{-1} \cdot K^{-1}$
S	Sorption coefficient	$L^3 \cdot M$
t	time	h
T	Temperature	°C
T_{dew}	Dew point temperature	°C
T_g	Glass transition temperature	°C
V_m	Molar volume at normal conditions	$m^3 \cdot mol^{-1}$
$V_{perm\ tank}$	Volume of the permeate tank	m^3
x	Fraction	

Greek Letters

α	Ideal selectivity	
β	y-intercept of Robeson upper bound	
θ_R	Robeson index	
θ	Bragg's angle	°
λ	X-ray wavelength	nm
Φ_v	Seep gas flow	$m^3 \cdot s^{-1}$

Indexes

0	Component 1
1	Component 2
A	Component A
B	Component B
i	Component i
j	Component j
perm	Permeate

List of Acronyms

ATR	Attenuated Total Reflection
CEM	Controlled Evaporation and Mixing
CMSM	Carbon Molecular Sieve membranes
DMSO	Dimethyl Sulfoxide
EDS	Energy Dispersive Spectroscopy
FFV	Fractional free volume
FTIR	Fourier Transform Infrared Spectroscopy
GC	Gas Chromatograph
IEA	International Energy Agency
IRENA	International Renewable Energy Agency
IUPAC	Union of Pure and Applied Chemistry
SEM	Scanning Electron Microscopy
SR	Shrinkage
TGA	Thermogravimetric Analyses
XRD	X-ray Diffraction

1 Introduction

1.1 Framing and presentation of the work

At present, the average Earth's temperature is already 1.1 °C higher than it was in the late 19th century, and greenhouse gas emissions have been increasing persistently. In order to limit global warming to a maximum of 1.5 °C above pre-industrial levels, as stipulated in the Paris Agreement, a 45 % reduction in gas emissions is necessary by 2030 and net-zero emissions should be reached by 2050 [1, 2].

Of the 50 billion tonnes of greenhouse gas emissions per year, more than 20 % comes from the transport sector (including aviation and maritime shipping) [3, 4]. With the world's population on the rise and income levels increasing, it is inevitable that all sectors of the economy will experience an expansion. The International Energy Agency (IEA) anticipates a doubling of global transportation, a 60 % rise in car ownership rates, and a threefold surge in demand for passenger and freight aviation by the year 2070 [5]. If it continues with only the current technologies, a very large increase in transport emissions will occur.

Figure 1.1 shows an optimistic scenario for the future of the transportation sector. To achieve this decrease in emissions, new and scalable technologies are needed. While electrification and hydrogen offer a promising approach to decarbonize light-duty transport, the use of these technologies becomes particularly challenging when it comes to heavy-duty trucking, maritime shipping, and aviation, primarily due to their high energy and power density demands. It is unrealistic to rely on batteries to power ships that must remain at sea for weeks or even months. One of the significant advantages of maritime fuel is that it can be of lower quality, more viscous, and less refined than those fuels employed in aviation or road transport. Moreover, it is possible to use the same existing infrastructures, including pipelines and bunkering [6].

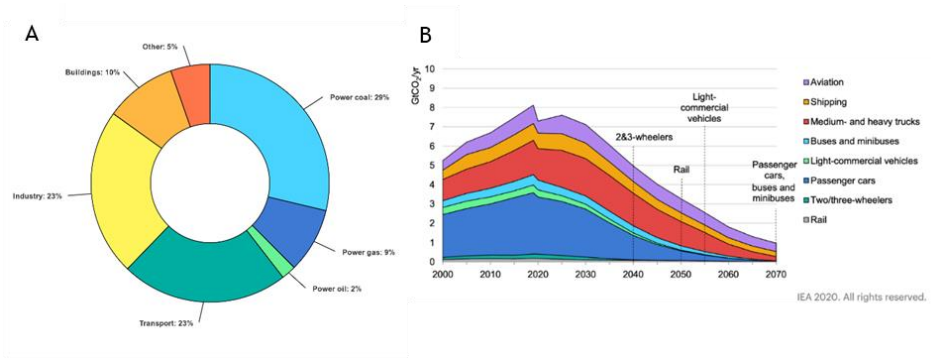


Figure 1.1. (**A**) CO2 emission by sector (reproduced from [3]); (**B**) Sustainable development scenario for transport emissions until 2070 (reproduced from [5]).

Liquid biofuels and e-fuels can be an excellent solution in this field, helping to decrease or even replace the use of fossil fuels. A biofuel is any fuel that is derived from biomass; while e-fuels, such as e-methanol, are generated from renewable electricity. They involve the production of green hydrogen and the direct capture of CO_2 from the atmosphere or industrial plants (e.g. biomass combustion) [7].

In 2021, IRENA (International Renewable Energy Agency) and Methanol Institute presented a report with some expectations about the present and the future of methanol. According to them, around 98 Mt of methanol are produced per year, but less than 0.2 Mt is renewable methanol, mostly bio-methanol [8]. To meet the Paris Agreement, this number needs to increase.

Renewable methanol, like e-methanol is made from the reaction of green hydrogen with renewable carbon dioxide and carbon monoxide. Hydrogen can be produced from renewable electricity and CO_2 from biomass [9]. Nowadays, the production cost for this type of methanol can range from USD 800-2,400 /t. However, as the prices of renewable hydrogen and CO_2 get lower, it is expected to decrease to USD 250-630 /t by 2050, which is a much more attractive cost [8].

Beyond its significant potential as a fuel, either as an additive, blend, or a replacement for fossil fuels, methanol finds various other applications, such as in the manufacturing of chemicals like acetic acid, dimethyl ether, alkenes and formaldehyde which are used in several products including paints, adhesives, plastics, and more [10].

Capwatt is currently working on a project to produce renewable methanol for fuel applications (**Figure 1.2**). The goal is to generate an annual output of 40,000 tons of methanol. To achieve this, the company plans to obtain hydrogen through water electrolysis, with the necessary electrical energy coming from a solar park, while capturing approximately 70,000 tons of CO_2 per year from biomass gasification. Carbon dioxide and hydrogen are introduced into a catalytic reactor, operating at a pressure of approximately 40 to 90 bar and a temperature range of 200 to 300 °C.

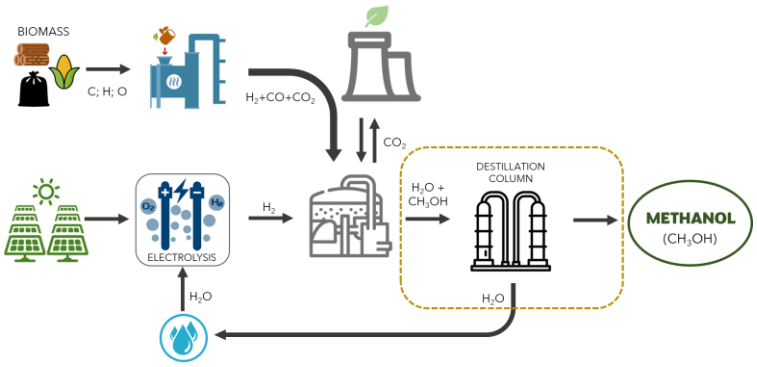


Figure 1.2. Scheme of Capwatt's methanol production process.

The reaction between carbon dioxide and hydrogen produces not only methanol, but also generates water as a byproduct [11]. It is necessary to remove the water, which is typically done through a distillation tower [12]. However, this process has an azeotropic limit which means that at the end, methanol is not pure enough. Further dehydration process with pressure swing absorption is necessary. These conventional methods consume large amounts of energy, are inefficient and difficult to maintain, and have a large carbon footprint, making the price of renewable methanol very high compared to fossil fuels [13].The goal for this project is to find and test a sustainable technology capable of withstanding severe conditions such as the temperature at the reactor outlet (>280 °C).

Membrane technologies are recognized as an energy efficient and environmentally friendly alternative for separation of gases and solvent mixtures [14]. Among the various types of membranes, carbon molecular sieve membranes (CMSMs) are one of the most promising porous inorganic membranes due to their simple manufacturing process and at the same time their excellent performance and stability under harsh conditions [15].

The objective of this work was to prepare hydrophilic carbon molecular sieve membranes for dehydration of alcohols. In addition to characterizing the membranes chemically and morphologically, the aim was also to test their performance in single gas separations and water/solvent mixtures separations.

1.2 Presentation of the companies

Capwatt was founded in 2008, leveraging the existing know-how of the Sonae Group. It is a company focused on developing and implementing more efficient and sustainable energy solutions that maximize synergies between decentralized production. Currently, Capwatt operates in Portugal, Mexico, and Spain, with over 90 projects in cogeneration, photovoltaic, wind, biomass, biogas, and energy storage technologies.

This project was carried out also in collaboration with CARBOPORA, a 2021 founded start-up from the Faculty of Engineering of the University of Porto. The company mission is to develop

and commercialize green, inexpensive, and renewable membrane-based separation solutions. Due to its university affiliation, it has a strong scientific and technological background, supported by more than 20 years of research and development experience in membrane separation technologies.

1.3 Contribution of the author to the work

During the initial weeks the author acquired the necessary skills to fabricate cellulose-based carbon molecular sieve membranes. Subsequently, the author produced carbon membranes with different boehmite content and different carbonization atmospheres in order to find the membrane with the best separation performances.

To analyze the performance of the membranes, the author conducted single gas permeation tests and prepared samples of each membrane for several characterization tests, performed by experts in the field.

Furthermore, the author actively contributed to the construction of an installation for testing water/solvent separations and then carried out the experiments using this setup.

The objectives outlined in this dissertation were successfully achieved within the planned timeframe.

1.4 Organization of the dissertation

This dissertation is divided into six main chapters, being chapter 1 a short introduction on the topic of green fuels and a presentation of the project companies' for this dissertation. Chapter 2 contains the important theoretical principles about membrane technology, principally about carbon molecular sieve membranes. Additionally, this chapter presents a state-of-the-art overview of membrane technology implemented in both gas separation and water/solvent separation processes.

The materials, characterization tests and the procedures utilized throughout this work are described in chapter 3. The results obtained with those methods are presented and discussed in the following chapter, the Results and Discussion chapter. Chapter 5 presents the conclusions of the work.

Finally, in chapter 6 an evaluation of the work is made both based on the accomplishment of the proposed objectives and on a personal evaluation of the work. The limitations found throughout the work and suggestions for future work are also presented.

2 Context and State of the art

2.1 Membranes

Membrane technology is currently a well-established technology in the market for separation processes, for example, for biogas upgrading [16] but it was only in the 80's that membranes started to be applied on industrial scale for gas separation processes [17].

Since then, a lot of innovation has been brought to this field, showing promising results. This technology has some great advantages like easy scale-up, possibility to combine with other technologies, continuous separation, low energy consumption and low operation and maintenance cost, becoming a very appealing technology for the future of the industry [18]. Especially, due to the need of various industries to separate carbon dioxide from gas streams, the gas separation membrane market has grown. In 2021, the global gas separation membranes market was valued at USD 0.9 billion and it is expected to grow up to USD 1.3 billion by 2027 [19].

A membrane (**Figure 2.1**) can be defined as a permselective barrier or an interface between two phases [20]. Basically, in this process, the feed stream, that is on one side of the membrane, is separated in two streams: the retentate and permeate streams. Depending on the final purpose of the separation, the required product will be in one of these streams. Certain components of the feed mixture are able to pass through the membrane due to the membrane's higher affinity for them. In order for this to happen, a driving force is necessary, which can be in the form of pressure, concentration, heat, or an electrical or chemical potential gradient established between the upstream and downstream [21, 22].

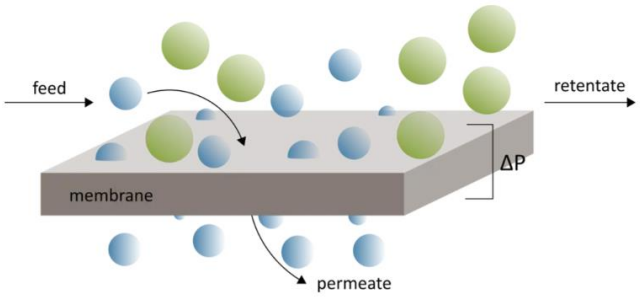


Figure 2.1. Scheme of membrane separation (reproduced from [22]).

Membranes can be classified regarding to their nature, structure or transport mechanism. Based on their nature, a membrane can be biological or synthetic. For synthetic membranes, they can be further divided into organic (polymeric), inorganic, or a mixture of these two types. International Union of Pure and Applied Chemistry, IUPAC, classify the structure of membranes according to the pore dimension [23], as described in **Figure 2.2**.

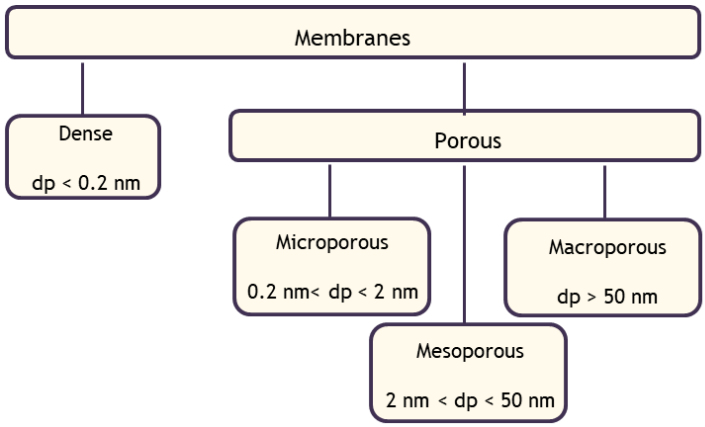


Figure 2.2. Membrane classification according to the pore size.

The structure of porous inorganic membranes can be classified as symmetric and asymmetric [18]. The structural differences are illustrated in **Figure 2.3**.

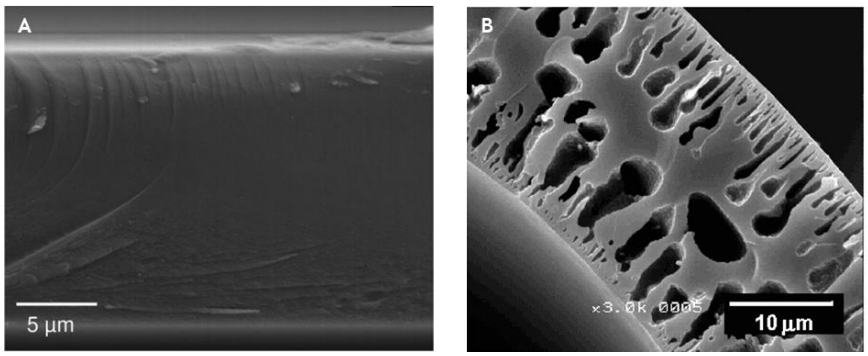


Figure 2.3. (**A**) symmetric structure (reproduced from [2]); (**B**) asymmetric structure (reproduced from [24]).

To date, polymeric membranes have held a prominent position in the global membrane market, primarily due to the availability of cost-effective polymer materials that exhibit favorable separation performance [18]. Cellulose acetate, polyacrylonitrile and polyethylene are some examples of materials used in these membranes [25]. Depending on the operating conditions, polymeric membranes can be glassy (hard and rigid), when the polymer is below its glass transition temperature, T_g, or rubbery (soft and flexible) [18], when the polymer is above its T_g. In the glassy state, the permeability tends to be lower and the selectivity higher than in rubbery state.

The major problem of polymeric membranes is their inability to withstand harsh conditions. When exposed to elevated temperatures and high levels of feed and water, they tend to swell, resulting in reduced effectiveness when separating biofuels [26]. There is also a trade-off between permeability and selectivity that this type of membranes cannot overcome – the so-

called Robeson Upper Bound [27]. Some of the leading players in the polymeric membranes market are DuPont, Air liquids, Evonik and Air products [28].

Inorganic membranes are a very promising alternative to overcome the limitations described above. Zeolites, silica and carbon membranes are included in this type of membranes. One of the major benefits of these membranes is their ability to withstand high concentrations of feed and water without swelling [14]. While zeolites can exhibit excellent hydrothermal stability, their ability to selectively separate smaller gas molecules is limited. Additionally, scaling up their production poses a challenge due to the complexities involved in synthesizing crack-free zeolite films with no inter-crystalline pores [14, 29]. Although silica exhibits favorable results in terms of hydrogen separation, its performance is unsatisfactory regarding selectivity and hydrothermal stability [14, 26]. Researchers are showing significant interest in Carbon Molecular Sieve Membranes (CMSM) due to their ability to simultaneously achieve high permeabilities and selectivities while maintaining stability.

Mixed matrix membranes combine the advantages of inorganic and polymeric membranes. By integrating a solid phase into a polymer matrix, it becomes feasible to achieve high mechanical properties, better processability and the low cost associated with polymeric materials. However, this type of membranes still has some limitations inhibiting its commercialization such as the agglomeration of the solid or the lack of adhesion between phases [18, 30].

In polymeric membranes (organic), the transport of gases is based on the solution-diffusion mechanism. Initially, gas dissolution takes place at the interface of the membrane. Subsequently, the gas moves through the membrane, transferring from one free volume to another and interacting with polymer chains. The final stage involves the gas being released at the opposite interface [29].

In contrast, in gas separation on a carbon membrane, there are four different separation mechanisms, depending on the size of the pores: Knudsen diffusion, capillary condensation, surface diffusion and molecular sieving [29]. The prevailing mechanism in a membrane depends on several factors, including the membrane's properties, the gases to be separated, and the operating conditions (such as temperature and pressure) [31]. Knudsen diffusion takes place when the pore diameter is smaller than the mean free path of the gas molecule, this mechanism is predominant in larger pores [32]. Capillary condensation can happen when the pore size is sufficiently small and a condensable penetrant can thoroughly wet the surface of the pore, leading to the formation of multiple layers of the penetrant molecules and to the filling of the pore [33]. The surface diffusion mechanism involves the adsorption of gas molecules at the entrance of a membrane pore, their subsequent migration along the pore’s surface, and their desorption at the other end [34]. Molecular sieving occurs when the pores are very small,

approaching the molecular dimensions of the species being absorbed which contributes to high selectivity [35]. **Figure 2.4** has a representation of the referred mechanisms.

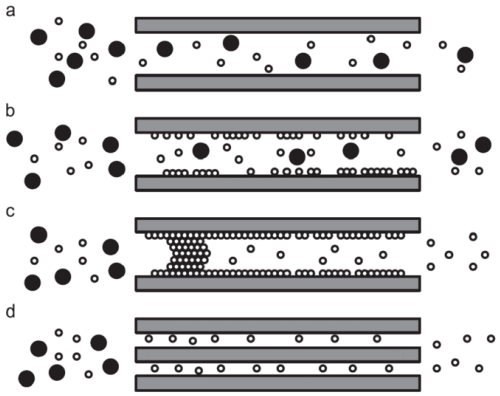


Figure 2.4. Transport mechanisms through a porous membrane: (**a**) Knudsen diffusion; (**b**) surface diffusion; (**c**) capillary condensation; (**d**) molecular sieving (reproduced from [36]).

Typically, a membrane performance is evaluated by two key factors: permeability, which reflects the membrane's productivity, and it is normally characterized by the flux trough the membrane, and selectivity, which measures the membrane's efficiency. A good separation process requires achieving good permeability and selectivity results, simultaneously [29].

The flux or permeation rate, *J*, is the flow through the membrane per unit area and it can be described by Fick's first law [37], as shown in Equation 1:

$$J = -D\frac{dc}{dx} \tag{1}$$

where D is diffusivity and $\frac{dc}{dx}$ is the driving force, that in this case is described as the concentration gradient, but it can be other driving force as previously mentioned. Being *l* the membrane thickness and integrating the previous equation between the upstream (high pressure) and downstream (low pressure) side, at the steady state, it is possible to obtain the following equation:

$$J = D\frac{c_0 - c_1}{l} \tag{2}$$

where $c_0 - c_1$ is concentration gradient. In case the solubility of the gas follows Henry's law [38]:

$$c = Sp \tag{3}$$

where *p* is the pressure of the gas and *S* the sorption coefficient, the proportionality constant. Combining Equation 2 and 3:

$$J = SD\frac{p_0 - p_1}{l} \tag{4}$$

where $p_0 - p_1$ is the pressure difference between the feed and the permeate side.

The Sorption-Diffusion model describes the membrane permeability, *P*, as the product of diffusivity (kinetic factor), and sorption coefficient (thermodynamic factor) [39], as shown in Equation 5:

$$P = DS \tag{5}$$

Therefore, the membrane permeability can be represented as,

$$P = \frac{Jl}{p_0 - p_1} \tag{6}$$

Usually, the unit of permeability is expressed in Barrer, where 1 Barrer is equal to 3.39 x 10^{-16} mol·m·m^{-2}·s^{-1}·Pa^{-1} [40].

The membrane efficiency is determined by the ideal selectivity, $\alpha_{A/B}$, that is defined as the ratio of the permeability of two pure gases [41], measured separately under the same conditions (Equation 7).

$$\alpha_{A/B} = \frac{P_A}{P_B} = \frac{D_A S_A}{D_B S_B} \tag{7}$$

As mentioned before, polymeric membranes suffer from a major limitation regarding to their trade-off between permeability and selectivity. Robeson [27] in his studies showed that there exists an intrinsic experimental upper bound limit, known as Robeson upper bound for the separation performance, as shown in **Figure 2.5**.

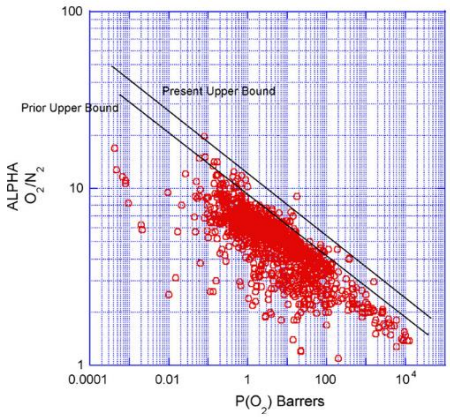


Figure 2.5. Robeson upper bound for O_2/N_2 separation (reproduced from [27]).

Contrary to polymeric membranes, CMSMs are not limited by the Robeson upper bound, being able to achieve a better balance between permeability and selectivity, surpassing the upper bound limit [42]. To quantify this performance, Araújo *et al*. [42] have proposed a new metric called the Robeson Index. This index is defined as the ratio between the actual selectivity value

($\alpha_{i,j}$) and the one corresponding to the Robeson upper bound ($\alpha_{i,j|RUB}$), both for a given permeability. The authors describe the Robeson Index as Equation 8:

$$\theta_R = \frac{\alpha_{i,j}}{\alpha_{i,j|RUB}} = \frac{\alpha_{i,j}}{k^{-\frac{1}{a}} P_i^{\frac{1}{a}}} = \frac{1}{\beta}\frac{\alpha_{i,j}}{P_i^m} \quad (8)$$

Where P_i is the permeability of the fastest gas, k is the "front factor", a is the slope of the log-log relationship, m is the slope of the Robeson upper bound for the gas pair and β is the y-intercept of the Robeson upper bound [42]. Essentially, the Robeson Index indicates how many times the membrane's performance exceeds Robeson's upper bound limit. If the performance is above or below this limit, the value of θ is greater than 1 or less than 1, respectively.

2.2 Carbon Molecular Sieve Membranes (CMSMs)

CMSMs are prepared by pyrolysis of a polymeric precursor. The initial stage involves selecting and preparing the precursor, followed by carbonization of the polymer membrane to form a carbon membrane. Prior to and subsequent to carbonization, the membrane can be subjected to pre-treatments and post-treatments, respectively [29].

The carbonization is performed under controlled conditions of atmosphere (*e.g.*, vacuum, N_2, Ar or CO_2) and temperature history. During the carbonization, the polymer decomposes, and the heteroatoms are released. This leads to the formation of carbon domains of randomly stacked sp^2 hybridized carbon sheets and sp^3 hybridized amorphous carbon [43]. Pores are created from packing imperfections between microcrystalline regions in the material [44]. This results in a carbon material with a CMSM structure that is described as turbostratic and "slit-like", featuring a bimodal pore size distribution with micropores connecting ultramicropores [2] (**Figure 2.6**).

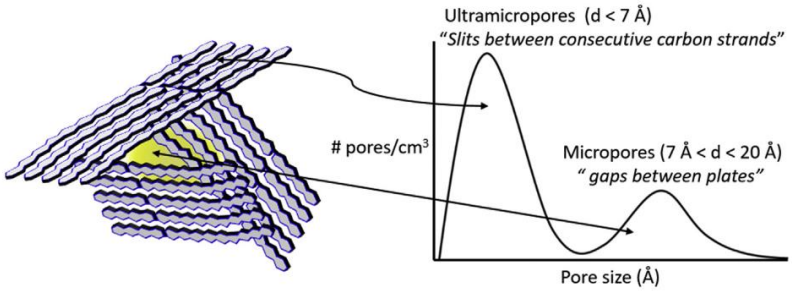


Figure 2.6. Turbostratic structure of a CMSM (reproduced from [45]).

While micropores provide sorption sites responsible for the surface diffusion, ultramicropores, called constrictions, allow molecular sieving. This combination results in high permeability and high selectivity, a very distinct characteristic of this type of membranes [2, 44].

One of the main problems of CMSMs was, until recently, their poor stability in certain environments and consequent membrane aging. In the presence of humidity and because of the low affinity of water on carbon surfaces, hydrophilic functional groups attract water molecules, which can initiate adsorbate-adsorbate interactions and promote further adsorption via hydrogen bonding, resulting in clusters of multiple water molecules that block the constriction [2, 46]. When the membrane is exposed to air, it occurs oxygen chemisorption [46], that also contributes to the reduction of porosity. Overcoming these challenges, Mendes group reported humidity-insensitive cellulose-based CMSM [2] and a stabilization procedure (post-treatment of the membranes with propylene) [47] that makes CMSM fully stable when in contact with air. Furthermore, it is still challenging to develop ultrathin and defect-free CMSMs. It was only in the 1980s that Soffer and Koresh become pioneers when they successfully prepared CMSMs by pyrolysis of organic precursors [48].

Carbon membranes can be either self-supported in the form of flat membranes, capillary tubes or hollow fibers, or they can be supported on flat or tubular structures using materials like metals, alumina or graphite. These different types of geometry can be seen in **Figure 2.7**. The microporous support appears to be a great solution to give mechanical stability to the membrane and overcome its brittleness; for that, the polymer solution can be deposited onto the support using various techniques including dip coating, spin coating, spray coating or even ultrasonic deposition [29].

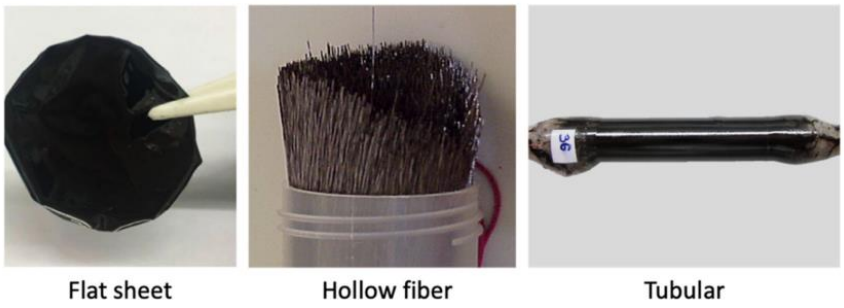


Figure 2.7. Different geometries of CMSMs (reproduced from [42]).

The choice of the polymer precursor is very important to obtain a stable CMSM. Besides its chemical structure, decomposition temperature, glass transition temperature and fractional free volume (FFV) are very important properties to achieve a good membrane structure and separation performance [29, 49]. Thermosetting polymers are being used due to their favorable characteristics under carbonization temperatures. Within the wide range of polymers, polyimides, polyetherimide, phenolic resins, polyacrylonitrile, polyphenylene oxide and cellulose are some examples of precursors used to produce carbon membranes [25].

2.3 CMSMs for gas separation

Over the past decades, numerous research groups have extensively investigated CMSMs for gas separation processes, revealing promising results [2, 42, 50, 51]. Among the different types of precursors mentioned in the previous chapter, polyimides are one of the most developed and promising precursors due to their high thermal stability, commercial availability and ease of processing the membrane [51, 52]. Researchers commonly use commercially available polyimides such as Matrimid, Kapton (Dupont), and P84 co-polymer. Researchers such as Fuertes *et al.* [51] and Tin and his colleagues [52] have conducted studies using these type of polyimides as precursors.

Due to the high production cost associated with polyimides, cellulose polymers are gaining importance. Cellulose, which is the most abundant organic compound on Earth [53], is continually replenished by nature, making it an inexpensive and almost limitless resource. In addition to being biodegradable, it has a significant carbon yield and hydrophilic and thermosetting properties, making it an excellent precursor to produce CMSMs [2, 42]. The strong hydrogen bonds between the molecular chains make it difficult to dissolve cellulose in conventional solvents. Moreover, conventional solvents may be toxic and harmful to the environment. To overcome this challenge, researchers are focusing on ionic liquids that besides having excellent dissolution ability, are easy to recycle, exhibit high thermal stability and have low propensity for crystallization [2].

Rodrigues *et al.* [2], used an ionic liquid to dissolve cellulose and prepare a cellulose based CMSM. According to the authors, this was the first study of CMSM produced from a cellulose precursor processed from ionic-liquids. After coating, the polymeric films were coagulated and washed in distillated water and then dipped in a bath containing propylene glycol. The polymeric membrane was subjected to pyrolysis at two different temperatures, 550 °C (CMSM 550) and 600 °C (CMSM 600). The membrane prepared at 550 °C end temperature exhibits a permeability to O_2 of 5.16 barrer and 0.16 barrer to N_2, and the membrane prepared at 600 °C showed a permeability to O_2 of 2.19 barrer and 0.09 barrer to N_2. Regarding O_2/N_2 ideal selectivity, CMSM 550 demonstrated a result of 32.3 and CMSM 600 of 24.3. An experiment was also performed in the presence of humidity (water vapor) which revealed higher permeability levels for humidified oxygen and nitrogen in CMSM 550 and CMSM 600, revealing that the presence of water molecules did not impair the separation. Humidified gas experiments are crucial as they provide an indication of water permeation. Although carbon membranes are normally hydrophobic, this team has shown that their membranes permeate water molecules, which is a very promising result that leaves expectations for the work of this dissertation.

In another study, Araújo *et al.* [54] prepared carbon membranes using a cellulose precursor regenerated from a ionic liquid with a 0.1 wt. % of boehmite ceramic nanoparticles. Boehmite

nanoparticles help to control the shrinkage of the precursor film during carbonization due to the formation of well-distributed nanowires within the carbon matrix. The results revealed a decrease in shrinkage in membranes with boehmite. The absence of boehmite resulted in a H_2 permeation of 305 barrer and a H_2/CH_4 permselectivity of 207 in the membranes, whereas the presence of boehmite increased the H_2 permeability to 530 barrer and the H_2/CH_4 permselectivity to 473. All gas experiments demonstrated an increase in both permeability and selectivity, indicating great potential for the utilization of these ceramic nanoparticles.

In 2021, Poto *et al.* [50] had already come to the conclusion that, due to the hydrophilicity of boehmite, the water adsorption into the porous carbon matrix increased, improving the water vapor permeation. In this work, supported CMSMs were prepared from a phenolic resin loaded with hydrophilic boehmite that was carbonized at 500 °C. The boehmite content was varied between 0.4 to 1.4 wt. %. The amount of water adsorbed increased with the boehmite content up to a maximum around 1 wt. %. Furthermore, the alumina content did not show significant effect on the pore distribution, but the thickness of the carbon layer increased as boehmite content increased, which was attributed to the rise in viscosity. The permeation test was conducted at high temperatures (150-250 °C) and among all the membranes, the one with 0.8 wt. % of boehmite content showed the best equilibrium between permeability and perm-selectivity.

2.4 Water/solvent separation with membrane technology

The state of the art for the vapor phase separation of water and alcohols such as methanol and ethanol using membrane technology is not very broad. Usually, this separation is done by pervaporation where basically a liquid stream containing two or more components is feed to the membrane and on the other side, vacuum or gas purge is applied [26].

In relation to water/alcohol separation using polymeric membranes, Ong and his colleagues [55] thermally rearranged a polyimide membrane, this technique allowed to obtain a permeance of 2.37 $mol \cdot m^{-2} \cdot h^{-1} \cdot kPa^{-1}$ and a selectivity of 186. Polyarylether membranes are also an example of polymeric membranes used for ethanol and methanol dehydration, as evidenced by Xu *et al.* [56], who obtained a permeability of 0.322 $mg \cdot m^{-1} \cdot h^{-1} \cdot kPa^{-1}$ for ethanol and 0.171 $mg \cdot m^{-1} \cdot h^{-1} \cdot kPa^{-1}$ for methanol, while the results for water/ethanol and water/methanol selectivities were 685 and 89.7, respectively.

Zeolites and silica are one of the most studied types of inorganic membranes. One of these works was performed by Sommer and Melin [57] that carried out a pervaporation test with different commercial tubular inorganic membranes. For ethanol and methanol dehydration tests performed at 70 °C, the ECN silica provided higher water permeance but lower selectivity than Mitsui zeolite T. Within zeolites, Zhang and Liu [58] produced high quality NaA zeolite

membranes supported on a porous metal sheet and performed water/ethanol separation, showing a selectivity greater than 10,000 and a permeation flux of about 4 $kg \cdot m^{-2} \cdot h^{-1}$.

Ueno et al. [59] achieve great performance results using a silicalite-1 zeolite membrane on tubular silica supports. The experiments were performed at a temperature of 50 °C, achieving a permeation flux of 4.47 $kg \cdot m^{-2} \cdot h^{-1}$ and a selectivity of 66. More recently, Peng *et al.* [60] prepared silanol-free hollow fiber MFI zeolite membranes for water/ethanol pervaporation and concluded that at 60 °C, the permeation flux was 2.81 $kg \cdot m^{-2} \cdot h^{-1}$ with a selectivity of 32. It was only more recently that pervaporation works with CMSMs started to appear, showing comparable or even better results than other types of membranes.

In 2010, Tin *et al.* [26] carried out a study for the dehydration of ethanol where they used a supported CMSM by an alumina tube and a polyimide (Matrimid) as precursor. The composite polymeric membranes were subjected to carbonization at 650 °C. The results obtained showed a separation factor of 50, a total flux of 4 $kg \cdot m^{-2} \cdot h$ and a water permeance of 223.22 $g \cdot m^{-2} \cdot h^{-1} \cdot kPa^{-1}$ at a feed temperature of 60 °C. The team also realized that an increase of the pyrolysis temperature has negatively affected the separation.

Later, Ngamou and his colleagues [14] produced ultrathin and defect free CMSMs supported in alumina tubes and using a polyimide precursor. The pyrolysis was carried out up to 700 °C. The group obtained very good results for both hydrogen purification and pervaporation of organic solvents. At 200 °C, the membranes showed a H_2 permeance of 1.1 x 10^{-6} $mol \cdot m^{-2} \cdot s^{-1} \cdot Pa^{-1}$ and ideal separation factors of 24, 130 and 228 for H_2/CO_2, H_2/N_2 and H_2/CH_4, respectively. The pervaporation was performed, at 70 °C, in a feed containing 90 wt. % of methanol or ethanol that resulted in a separation factor of 791 and 1,946, respectively, and a water flux of about 0.5 $kg \cdot m^{-2} \cdot h^{-1}$.

A tubular supported CMSM using Novolac oligomer phenolic resin as precursor was produced by Rahimalimamaghani and his team [61], for ethanol dehydration. The experiment aimed to investigate how the polymerization time and the pulling speed during the dip coating step affected the water permeance and selectivity. The most optimal balance between these two factors was achieved using an alumina support, longer oligomer reaction time, and higher pulling speed, resulting in a water flux of 1.1 $kg \cdot m^{-2} \cdot h^{-1}$, water permeance of 4.65 $mol \cdot m^{-2} \cdot h^{-1} \cdot kPa^{-1}$ and a selectivity of 664. Still in this field, in 2022, Yoon and Lively [39] studied a model for the mechanism of permeation of water and p-xylene in carbon membranes demonstrating the potential of this type of membranes for the removal of dilute organics in water.

Table 1 and **Table 2** summarize the most significant results of the studies presented above for possible comparison of the works.

Table 1. Comparison of pervaporation membranes applied to aqueous ethanol dehydration.

Membrane	Feed Temperature (°C)	Water concentration in feed (wt. %)	Pressure ratio (Pa)	Water Flux ($g \cdot m^{-2} \cdot h^{-1}$)	Water permeance ($mol \cdot m^{-2} \cdot h^{-1} \cdot kPa^{-1}$)	Mole-based selectivity	Ref.
Polymeric							
Chitosan (crosslinked with glutaraldehyde)	60	10	150	300	0.17	417	[62]
Thermally rearranged polybenzoxazole	25	10	100	5,694	3.16	186	[55]
H-PESU (polyarylether)	60	15	100	2,474	1.37	685	[56]
Inorganic							
ECN silica	70	10	1,400	2,330	1.31	60	[57]
Mitsui zeolite X	70	10	700	910	0.51	1,000	[57]
NaA zeolite (metal sheet support)	75	10	1,333	3,960	2.23	>10,000	[58]
Silicalite-1 (silica support)	50	10	Not available	4,470	-	66	[59]
W-MFI zeolite (hollow fiber)	60	5	200	2,810	1.56	32	[60]
CMSM							
CMSM-650 (tubular α-alumina support)	60	50	500	3,907	2.18	50	[26]
Carbon, tubular	70	10	1,000	542	0.30	1,946	[14]
$AlN_{10}M_{10}$	70	10	400	1,196	4.65	664	[61]

Table 2. Comparison of pervaporation membranes applied to aqueous methanol dehydration.

Membrane	Feed Temperature (°C)	Water concentration in feed (wt. %)	Test pressure (Pa)	Water Flux ($g \cdot m^{-2} \cdot h^{-1}$)	Water permeance ($mol \cdot m^{-2} \cdot h^{-1} \cdot kPa^{-1}$)	Mole-based selectivity	Ref.
Polymeric							
Chitosan (crosslinked with glutaraldehyde)	60	10	150	301	0.17	68	[62]
H-PESU (polyarylether)	60	15	100	1,314	0.72	89.7	[56]
Inorganic							
ECN silica	70	10	1,400	1,870	1.05	10	[57]
Mitsui zeolite X	70	10	700	270	0.15	100	[57]
CMSM							
Carbon tubular	70	10	10	529	0.30	791	[14]

In April 2023, Poto *et al*. [63] reported for the first time vapor/gas separation experiments through CMSMs. The permeation experiments were carried out at a temperature of 150-250 °C and they obtained a permeance of 1.15 $mol \cdot m^{-2} \cdot h^{-1} \cdot kPa^{-1}$ with a water/methanol selectivity of 4.3 at 200 °C.

The objective of this dissertation is to use unsupported cellulose based CMSMs to separate water and methanol through gas separation instead of pervaporation. Since the stream from the Capwatt's methanol reactor is at a temperature of 200°C, both components are in a gaseous state, making it advantageous for the company to separate them without the need to cool the process. This approach has not been explored before, highlighting the great significance of this work.

3 Materials and Methods

In this chapter are presented the materials and the process used to produce the CMSM. Several membrane characterization tests were performed to understand the chemical and physical structure of the CMSM, followed by permeation and separation tests. These are also described in this chapter.

3.1 Materials

The polymer used was raw cellulose provided by Innovia Films Ltd and consisting of wood pulp with a degree of polymerization of 450. The ionic liquid, 1-ethyl-3-methylimidazolium acetate (Emimac) (≥ 95 %), purchased from IoLiTec, was used to dissolve cellulose. Dimethyl sulfoxide (DMSO) was purchased from Fisher Scientific. For the samples with boehmite, AlO(OH), a dispersion of boehmite nanoparticles (10 %) was used, with particle size 8-20 nm named *Alumisol* and provided by Kawaken Fine Chemicals Co. Ltd. Air Liquide supplied the various gases needed for the work, namely hydrogen (99.999 %), carbon dioxide (99.998 %), nitrogen (99.999 %) and oxygen (99.995 %). The 70 vol. % ethanol solution was provided from Valente e Ribeiro. LDA and Sigma-Aldrich supplied methanol (99.8 %).

3.2 Preparation of cellulose precursor membranes

The composite polymeric precursor solution was prepared by dissolving cellulose (9.2 wt. %) in a solution of DMSO and Emimac 70:30 wt. % ratio, respectively, and adding the boehmite dispersion into the mixture. Four different solutions were prepared: one without boehmite and the others containing 0.55, 1.10 and 2.15 wt. % of boehmite in relation to cellulose. The solution was heated at 90 °C under magnetic stirring until the cellulose was completely dissolved, that is about 2 h. After the dissolution, the solution needs to settle for 2 h to remove any trapped air bubbles. The resultant solution exhibits a brownish color and a viscous rheology.

The polymeric films were prepared in rectangular glass plates in a spin coater (POLOS™, SPIN150i) at a spinning speed of 1,000 rpm with an acceleration of 1,000 rpm·s^{-1} for 10 s. After coating the films were immediately coagulated in distilled water at room temperature and washed with distilled water for 1 hour to remove the excess of ionic liquid. The films were dried overnight under ambient conditions.

3.3 Preparation of cellulose based CMSMs

Before the carbonization step, the dried precursor films were cut into disks with 58 mm diameter and placed in a horizontal stainless-steel grid. The carbonization took place in a

quartz tube (80 mm in diameter and 1.5 m in length) inside a tubular Termolab TH furnace. To guarantee that the temperature is constant along the quartz tube, the furnace has three separating heating elements controlled by three PID control heating parameters. Different purge gases were utilized to test the influence of the atmosphere during the carbonization step. Carbon dioxide and nitrogen were used in a continuous flow rate of 170 $mL \cdot min^{-1}$, and nitrogen was used with 5 vol. % of hydrogen. The heating rate was 0.5 $^{\circ}C \cdot min^{-1}$, following the temperature history described in **Figure A.1** (see Appendix A). The several 30 minutes steps are necessary to avoid a quick release of residual solvents/volatile matter that could damage the carbon matrix, causing cracks or defects. After the end temperature (550 °C) was reached, the system was allowed to cool down until room temperature so that the membranes could be removed.

Table 3 describes the reference name of the different membranes as well as the various experimental conditions used in their preparation.

Table 3. Preparation conditions of the different CMSMs.

CMSM	wt. % of boehmite $\left(\frac{mass\ of\ boehmite}{mass\ of\ solids}\right)$	Carbonization atmosphere
CMSM 0	-	CO_2
CMSM 0.55	0.55	CO_2
CMSM 1.10	1.10	CO_2
CMSM 2.15	2.15	CO_2
CMSM CO_2	1.10	CO_2
CMSM N_2	1.10	N_2
CMSM N_2+H_2	1.10	N_2+ 5 vol. % H_2

3.4 CMSM characterization

3.4.1 Scanning Electron Microscopy (SEM) and Energy Dispersive Spectroscopy (EDS)

SEM produces micrographs of a sample by projecting and scanning a focused beam of electrons that interact with the sample, creating several signals that can be used to obtain information about the surface's structure and chemical composition by Energy Dispersive Spectroscopy, EDS [64]. The morphology features of the materials were evaluated by SEM, using a Hitachi TM4000 plus (Hitachi, Tokyo Japan) equipment. The samples were placed on a carbon tape and the microscope was operated using an applied voltage of 15 kV and a Backscattered Electron (BSE) detector. Additionally, the compositional mapping data was obtained by EDS.

3.4.2 Thermogravimetric Analysis (TGA)

TGA is used to determine the material's thermal stability and its fraction of volatile components measuring the mass of sample over time as the temperature changes. In this work, TGA tests were performed using a thermogravimetric balance (NETZSCH STA 449 F3 Jupiter) under 30 mL·min^{-1} continuous nitrogen flow, with a heating ramp from room temperature until 950 °C and a heating rate of 10 °C·min^{-1}. The goal was to understand how the polymeric film behaves during carbonization and to determine the corresponding mass loss. It was also possible to confirm the boehmite content of the membrane performing TGA under 30 mL·min^{-1} constant air flow from room temperature until 950 °C, with the same heating rate.

3.4.3 Fourier Transform Infrared Spectroscopy with Attenuated Total Reflection (FTIR-ATR)

Fourier transform infrared spectroscopy is an analytical technique used for characterizing the chemical structure (functional groups) of the sample. FTIR identifies chemical bonds and their characteristic vibrations by measuring the absorption of infrared radiation at different wavelengths. The wavelengths absorbed by the sample are characteristics of its molecular structure and can be identified by analysis of the resulting absorption bands [65]. ATR is based on total internal reflection where infrared light passes through the ATR crystal and interacts with the sample only at the point where the infrared light is reflected.

FTIR tests were performed using a VERTEX 70 FTIR spectrometer (BRUKER) in transmittance mode with a high sensitivity DLaTGS detector at room temperature. The samples were measured in ATR mode, with a A225/Q PLATINUM ATR Diamond crystal with single reflection accessory. The spectra were recorded from 4,000 to 500 cm^{-1} with a resolution of 4 cm^{-1}. In this work, FTIR technique was used to understand the effect of carbonization and if the addition of boehmite altered the chemical structure.

3.4.4 X-Ray Diffraction analysis (XRD)

XRD analysis is a technique where a collimated incident beam of X-rays interacts with the electron clouds in the atoms of the sample and is diffracted at different angles originating a diffraction pattern. This technique provides valuable information about the crystallographic structure, chemical composition and physical properties of a material [64]. The structural characterization of the CMSMs was performed using a Rigaku SmartLabSe diffractometer (Cu Kα radiation – 1.5406 Å, 40 kV, 30 mA). The XRD patterns were collected in the range 7° < 2θ < 60°.

3.4.5 Raman spectroscopy

The principle of Raman spectroscopy lies on the inelastic scattering of photons from a laser in the sample, resulting in photons with altered energies compared to the incident light. In

contrast to FTIR, which measures the remaining light from the original light source, Raman spectroscopy measures the energy that scatters after being excited [65]. This technique was utilized to analyze the crystallinity of the samples and how boehmite influences the disorder of the structure. The Raman spectra of the CMSMs were obtained using a WITEc alpha300 R Confocal Raman with an excitation wavelength of 532 nm.

3.4.6 Water contact angle measurements

Water contact angle measurement is a qualitative way to evaluate whether the surface has a hydrophobic or hydrophilic characteristic. The angle between the face of the solid surface and the tangent line to the contacting edge of the droplet is measured [66]. It was used a DATAPHYSICS goniometer, model OCA 15 with the SCA20 computer application, using the sessile drop method. During the test, the syringe deposits a drop of ultrapure water on the surface of the carbon membrane with a stipulated volume of 4 μL. Then the camera captures the drop and with the help of the computer application, the contact angle was determined. The angle was calculated from the tangent to the drop profile at one-second intervals over a duration of two minutes.

3.5 Gas permeation test

Prior to the single gas permeation tests, the carbon membrane was glued with epoxy glue (Araldite® rapid) to a circular stainless-steel disc, with a 10 mm diameter hole in the center, to prevent them from breaking when assembled into the permeation cell. The glue was also applied along the interface of the stainless-steel support/CMSM and then allowed to dry for 2 h. Finally, it was covered with filter paper.

Single gas permeation tests were performed inside a thermostatic cabinet, as its possible to see in **Figure A.2** and **Figure A.3** (see Appendix A). The temperature was maintained at 25 °C with a feed pressure of 1 bar and the permeate pressure was about 0.02 bar. The membrane cell was connected to two separated tanks, one to the permeate side and the other to the feed side. On batch experiments with dry feed gas, the feed tank was filled before feeding the cell, while continuous experiments with humidified feed gas were performed by passing a portion of the gas stream through a distilled water bubbler to reach 80-90 % of relative humidity. Permeation of H_2, CO_2 and O_2 was conducted for 1 h while permeation of N_2 and humidified N_2 was carried out overnight. A digital high-accuracy micrometer from Mitutoyo MDH-25M was used to determine the CMSM and precursor film thickness. The permeability, *P*, of the species was determined accordingly to Equation 6 and was computed from the experimental data as follows:

$$P = \frac{\delta \, V_{perm\,tank} \, V_m \Delta P_{perm}}{R \, T \, t \, A_{cell} \, (p_{feed} - p_{perm})} \tag{9}$$

where $V_{perm\,tank}$ is the volume of the permeate tank, V_m is the molar volume of the gas at normal conditions, R is the gas constant, T is the absolute temperature, t is the time, A the working area of the flat carbon membrane and ΔP_{perm} is the permeate pressure increment for the time t. Selectivity was determined with Equation 7.

3.6 Water/solvent separation tests

Prior to the water/solvent separation tests, the carbon membrane was once again glued to a circular stainless-steel disc, with a 10 mm diameter hole in the center, but this time a high-temperature resistant J-B Weld™ glue was used, that can withstand temperatures up to 280 °C. The glue was also applied along the interface of the stainless-steel support/CMSM and then allowed to dry overnight. Before introducing the carbon membrane into the module, it was protected with filter paper.

The installation that was constructed for the initial water/solvent separation tests is presented in **Figure A.4** (see Appendix A) and in **Figure A.5** (see Appendix A) are showed some laboratory photographs. Firstly, the HPLC pump feeds the mixture to the membrane module that is inside an oven, where a heat exchanger heats the feed solution to the desired temperature for the respective test. While permeation is taking place, the retentate stream passes through a condenser and is recycled. The permeate stream was kept at a pressure of 20 mbar by means of a vacuum pump and collected in a cold trap, cooled with liquid nitrogen. To calculate the permeability, P, the liquid collected in the trap was weighed, being possible to use Equation 10,

$$P = \frac{m_{permeate}\, l}{M\, A\, t\, \Delta p} \tag{10}$$

where $m_{permeate}$ is the permeate collected mass, M corresponds to the water molar mass, A to the membrane working area, t to the experiment time and Δp to the pressure difference between the feed and the permeate side.

Later, a second approach to the installation was assembled, as is presented in **Figure 3.1**. The laboratory set up can be seen in **Figure A.6** (see Appendix A). In this case, a sweep gas (nitrogen) is connected to the permeate stream, lowering the water vapor partial pressure, creating the necessary driving force for the separation process. The carrier gas has also the function of carrying the permeate stream to a gas chromatograph (GC) to determine which components are present in the permeate stream. The GC used was a 2010 Plus from Shimadzu, equipped with a barrier ionization detector and a Pora-Plot Q (Agilent) column; N_2, from the sweep gas, was used as the carrier gas. GC runs were initiated 15 min after starting the experiments and subsequently performed every 10 min.

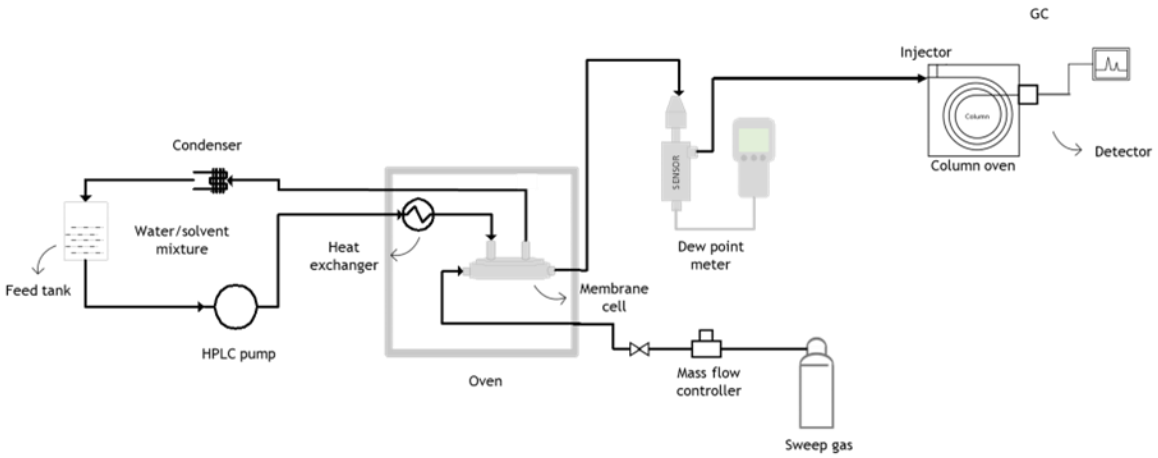


Figure 3.1. Experimental setup for water/solvent separation tests.

Since the GC only measures the components that permeated the membrane, but does not provide quantitative permeation values, the permeate stream was connected to a humidity sensor before reaching the GC, that reported the dew point temperature of the stream. With the dew point temperature it is possible to obtain the vapor pressure of the permeate and with the Antoine equation, the permeance by the method created by Metz *et al*. [67].

Those authors deduced the Equation 11 (see Appendix A) to calculate de permeance, P/l, where l is the thickness of the membrane, Φ_v is the flow rate of the sweep gas, $p_{H_2O,feed}$ and $p_{H_2O,perm}$ are the water vapor pressure of the feed and permeate side of the membrane, respectively, P_{tot} is the total pressure at the permeate side of the membrane and finally, A_{cell} is the membrane working area.

$$\frac{P}{l} = \frac{\Phi_v \ln\left(\frac{p_{H_2O,feed}}{p_{H_2O,feed} - p_{H_2O,perm}}\right)}{P_{tot}\, A_{cell}} \tag{11}$$

Equation 12 describes the Antoine equation, where the vapor pressure of the streams, p_{H_2O}, is given in bar and T_{dew} is the dew temperature (°C) of the respective stream. The water specific constants [68] used are given in **Table A.1** (see Appendix A).

$$log_{10}(p_{H_2O}) = A - \frac{B}{T_{dew} + C} \tag{12}$$

For the separation tests it was used the CMSM with 1.10 wt. % of boehmite, carbonized in a CO_2 atmosphere. Firstly, direct injections of 1 ppm of ethanol and methanol were conducted into the GC to observe their respective retention times. This allowed for differentiation of these components when mixtures of water and organic solvents were introduced. Subsequently, tests were performed, for 30 min of 50/50 vol. % methanol-water mixtures at 120 ºC and 200 ºC, and being of interest to the companies, a 70/30 vol. % ethanol-water test was performed at 120 ºC.

4 Results and Discussion

As stated in the previous chapter, CMSMs were prepared from cellulose precursors without boehmite and with 0.55, 1.10 and 2.15 wt. % of boehmite content in relation to cellulose, and they were carbonized in a CO_2 atmosphere. To study the influence of the carbonization atmosphere, CMSMs with 1.10 wt. % of boehmite were also prepared in carbonization atmospheres of N_2 and N_2 with 5 vol. % of H_2.

The results of the different tests are structured in three subchapters. Firstly, are presented the results of the characterization tests conducted on the various samples. Following that, the permeation test results are discussed and lastly, the water/solvent separation tests performed are described, as well as the respective results obtained.

4.1 Characterization tests

4.1.1 Preparation of CMSM

During the carbonization, the volatile compounds are released, the cellulose matrix decomposed, and a pore network is formed. **Figure 4.1** shows the polymer film and the corresponding carbon membrane after carbonization.

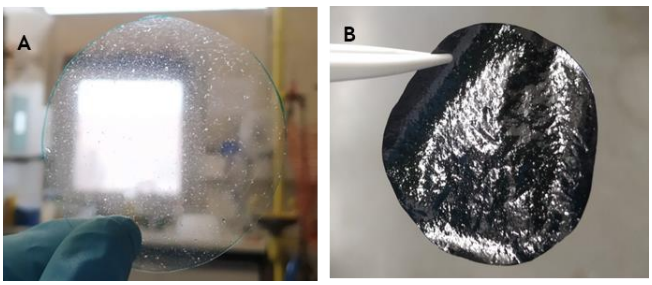


Figure 4.1. Cellulose membrane with boehmite nanoparticles (**A**) before and (**B**) after carbonization.

The diameter and thickness of the precursor and corresponding CMSM were measured to estimate the shrinkage of the polymer during carbonization. The results are shown in **Table 4**. The diameters of the seven different CMSM are very similar (between 40 and 41 nm), so the differences in diameter shrinkage are not significant. Concerning the thickness, the membranes produced with 0.55 and 1.10 wt. % of boehmite in a CO_2 atmosphere are the samples that exhibit lower shrinkage.

Table 4. Dimensions of the cellulose membrane before and after carbonization.

CMSM	Diameter (mm)			Thickness (μm)		
	Precursor	CMSM	SR (%)	Precursor	CMSM	SR (%)
CMSM 0	58.0	40.0	31.0	45.5	27.9	38.7
CMSM 0.55	58.0	41.0	29.3	42.7	28.1	34.0
CMSM 1.10	58.0	40.5	30.2	40.9	26.9	34.3
CMSM 2.15	58.0	41.0	29.3	50.5	27.1	46.1
CMSM CO_2	58.0	40.5	30.2	40.9	26.9	34.3
CMSM N_2	58.0	40.0	31.0	40.8	20.9	48.8
CMSM N_2+H_2	58.0	40.0	31.0	42.1	27.0	35.9

4.1.2 Scanning Electron Microscopy (SEM) and Energy Dispersive Spectroscopy (EDS)

The surface and cross-section morphology of polymer precursor samples and the respective carbon membrane were analyzed by SEM, as is presented in **Figure 4.2** and **Figure 4.3**. It was also performed EDS to the CMSMs to determine the mass percentage of each component (**Table 5**). The data presented in **Figure 4.2** and **Figure 4.3** clearly demonstrates that the surface of the samples is free from defects.

With an increase in boehmite content, the presence of boehmite nanoparticles becomes more prominent in both the normal plan and cross-section of the precursor and respective carbon membranes. In the cross-section images, it is possible to observe that there are no nanoparticles agglomerates meaning that the boehmite is well distributed. When examining the cross-section of the polymeric precursor films, it is observed that in the absence of boehmite, the structure appears denser. However, upon the addition of boehmite, the structure becomes more asymmetric. During the carbonization process, it appears that the pores collapse, resulting in a denser structure. Observing the mass fractions of the components, in **Table 5**, the increase in the amount of boehmite is demonstrated by the decrease of the C/O and C/Al ratios, since boehmite is an aluminum oxide hydroxide.

Regarding the carbonization atmospheres shown in **Figure 4.3**, it is possible to observe that the normal profile of the carbon membranes produced with 1.10 wt. % of boehmite and a carbonization atmosphere of nitrogen with 5 vol. % of hydrogen (**Figure 4.3C**) demonstrates more boehmite nanoparticles and, on other hand, with inert atmosphere, the nanoparticles are not so noticeable. This observation aligns with the results obtained through the EDS technique, where the reductive atmosphere resulted in a lower C/Al ratio, while the inert atmosphere yielded a higher ratio.

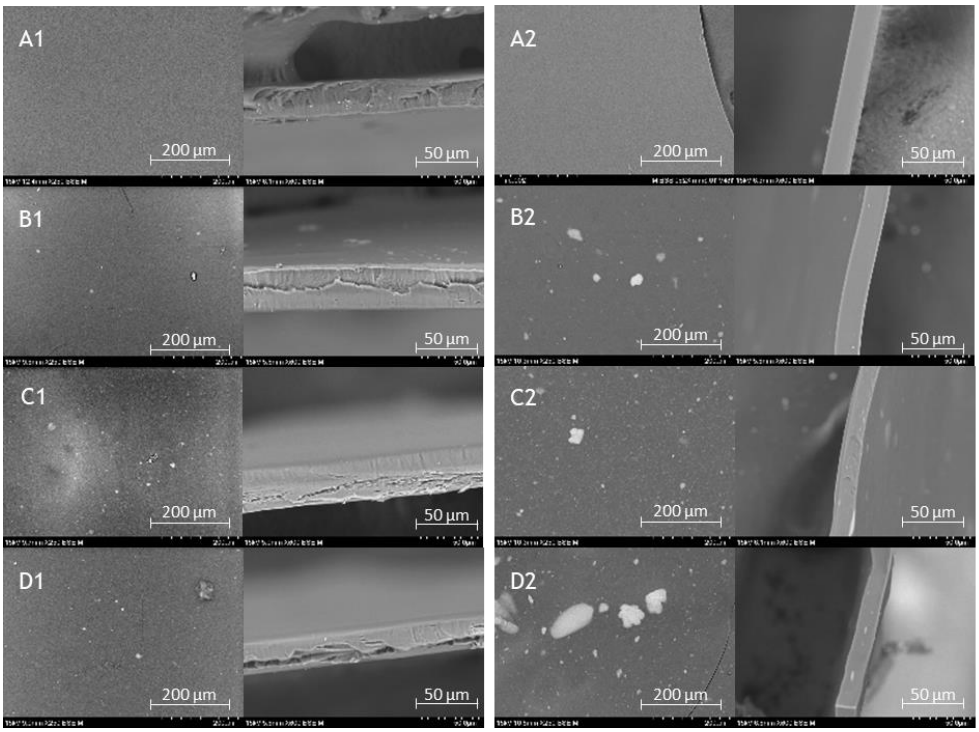


Figure 4.2. SEM images of the precursor film (**A1**) without boehmite and a boehmite content of (**B1**) 0.55 wt. %, (**C1**) 1.10 wt. %, (**D1**) 2.15 wt. % in normal plan (left) and cross section (right); SEM images of (**A2**) CMSM 0, (**B2**) CMSM 0.55, (**C2**) CMSM 1.10 and (**D2**) CMSM 2.15.

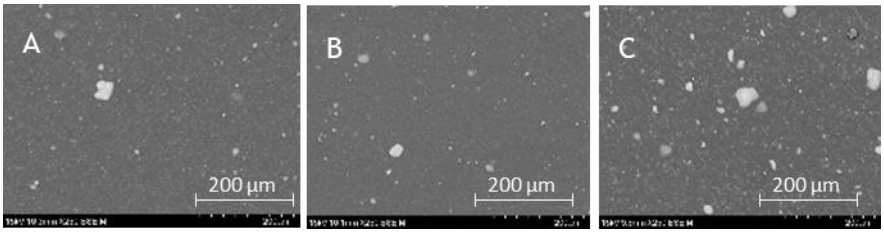


Figure 4.3. SEM images of (**A**) CMSM CO_2, (**B**) CMSM N_2 and (**C**) CMSM N_2+H_2.

Table 5. Mass percentage of the membrane composition given by EDS technique

		Mass C (%)	Mass O (%)	Mass Al (%)	C/O	C/Al
Polymeric film, 0 wt% boehmite		48.66	51.34	-	0.95	-
CMSM	CMSM 0	92.48	7.52	-	12.30	-
	CMSM 0.55	91.22	7.99	0.80	11.42	114.03
	CMSM 1.10	89.90	8.28	1.82	10.86	49.40
	CMSM 2.15	86.04	11.13	2.83	7.73	30.40
	CMSM CO_2	89.90	8.28	1.82	10.86	49.40
	CMSM N_2	90.79	7.51	1.70	12.09	53.41
	CMSM N_2+H_2	89.07	8.72	2.21	10.21	40.30

4.1.3 Thermogravimetric Analyses (TGA)

Thermogravimetric analysis was performed to evalute the thermal stability and decomposition kinetics of the cellulose precursor with boehmite nanoparticles. The mass loss curve of the polymeric films and the carbon membranes, subjected to a temperature of 550 °C and 950 °C, respectively, is represented in **Figure 4.4**. On the other hand, **Table 6** provides a summary of the significant findings extracted from the TG curves.

Until 150 °C (**Figure 4.4A**) all the water that was inside the polymeric film evaporates originating a decrease in mass up to this temperature. Between 200 °C and 380 °C there is a marked drop in the mass of the sample, which is due to the decomposition of the polymer, and the pore network begins to form and organize from this temperature on, along with further cellulose degradation. The derivative of TGA of precursor films, plotted in **Figure A.8** (see Appendix A), allowed to find out the temperature of maximum degradation. The addition of boehmite caused the polymer degradation to take place at a slightly higher temperature, proving that the inorganic load introduces stability to the membrane structure .

Focusing on the TGA experiments performed under oxygen flow until 950 °C, **Figure 4.4B**, there is a sligh increase in the mass (@ 300 °C) of the samples due to the formation of oxygenated groups that are then released. The gasification of the carbon membrane starts around 390 °C, and in the end, only the boehmite particles remain (inorganic matter). As expected, the final mass increases with the increase in the amount of boehmite in the membrane.

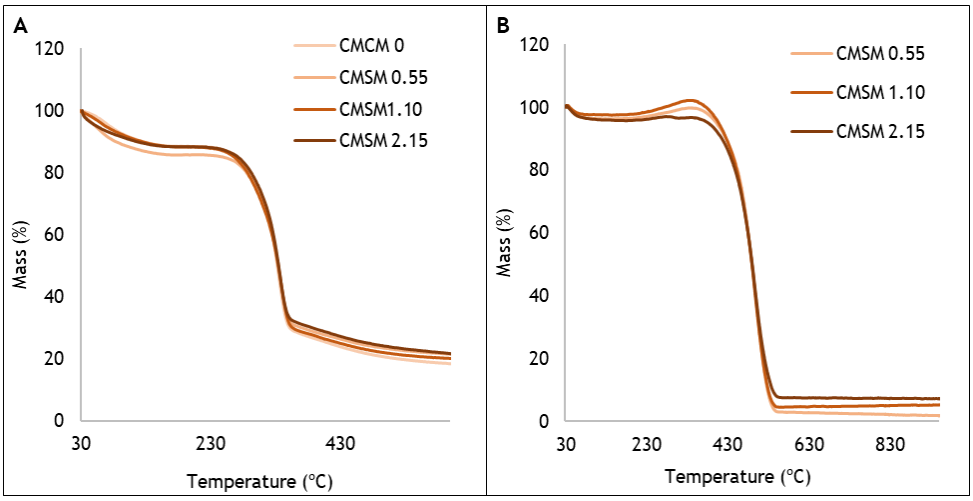


Figure 4.4. TGA of the (**A**) polymeric precursor and (**B**) the carbon membranes.

Table 6. Summary of the information obtained from TGA.

	0 B	0.55 B	1.10 B	2.15 B
Film mass loss at 150 °C (%)	11.1	13.9	11.2	13.1
Maximum degradation T (°C)	332.7	340.1	338.0	339.5
CMSM mass loss at 950 °C (%)	100.0	98.3	94.8	92.9

4.1.4 Fourier Transform Infrared Spectroscopy (FTIR)

The chemical structure of the polymeric films and the respective carbon membranes was examined through FTIR. **Figure 4.5** shows FTIR spectra of the precursor films and derived carbon membranes with different boehmite content. The bands assigned to the spectra displayed are summarized in **Table A.2** (see Appendix A).

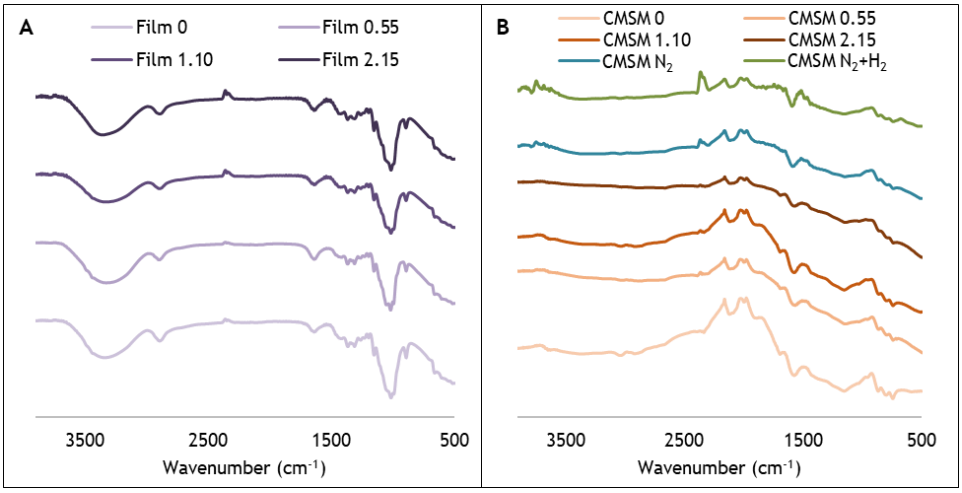


Figure 4.5. FTIR spectra of (**A**) the precursor films and (**B**) respective CMSMs.

The precursor spectra show a wide band at 3,350 cm^{-1} which is assigned to the O-H stretching in hydroxyl and carboxyl groups [69]. The aliphatic structures are deduced from the band 2,898 cm^{-1}, that corresponds to the stretching vibration of aliphatic C-H [69]. The band seen at 1,643 cm^{-1} appears in the region of the stretching vibrations of C=C and C=N and the deformation of the NH bond. CH_2 bending vibrations can be seen at 1,317 cm^{-1}; 1,159 cm^{-1} correspond to C-O-C stretching vibrations and 1,012 cm^{-1} to C-O stretching vibrations [70]. Finally, it is possible to find glycosidic linkages between glucose at 894 cm^{-1} [69].

After the carbonization, the band corresponding to O-H stretching, at 3,623 cm^{-1}, is less demarcated due to polymer decomposition [69]. In the carbon membrane is possible to identify =C-H stretching at 3,024 cm^{-1}; the aliphatic structures are deduced from 3,033 cm^{-1}. After pyrolysis the band corresponding to N≡C stretching is detected, at 2,123 cm^{-1}. At 2,001 cm^{-1}, the substituted benzene rings are identified [70] and at 1,643 and 1,573 cm^{-1} appear once again the bands recognized as the stretching vibrations of C=C and C=N and the

deformation of the NH bond. At 1,837 cm^{-1} the C=O stretching vibrations are observed, CH_2 bending vibrations are detected at 1,317 cm^{-1} and at 1,143 cm^{-1} is possible to observe C-O-C stretching vibrations [70]. Lastly, the 862 cm^{-1} and 788 cm^{-1} are assigned to aromatic C-H bending vibrations.

By comparing the spectra with no boehmite and with different quantities of boehmite, on both the polymeric film samples and the respective membranes, the OH band decreases as the boehmite content increases. The same happens in the intensity of the band characteristic of substituted benzene rings, at 2,001 cm^{-1}, and the N≡C stretching vibration are also less intense. When comparing the carbon membranes carbonized under different atmospheres, C-O-C stretching vibrations, at 1,143 cm^{-1} are slightly more intense when carbonizing with a CO_2 atmosphere.

4.1.5 X-Ray Diffraction analysis XRD

The interlayer distance (*d*-spacing) of the carbon membranes was evaluated by XRD. **Figure 4.6** shows the XRD spectra for the CMSMs and **Table 7** summarizes the *d*-spacing values, that were calculated using Bragg's equation:

$$d = \frac{n\,\lambda}{2\,sin\theta} \tag{14}$$

Where n is the diffraction order, λ is the X- ray wavelength, and θ is the angle between the incident ray and the diffracting planes (Bragg angle).

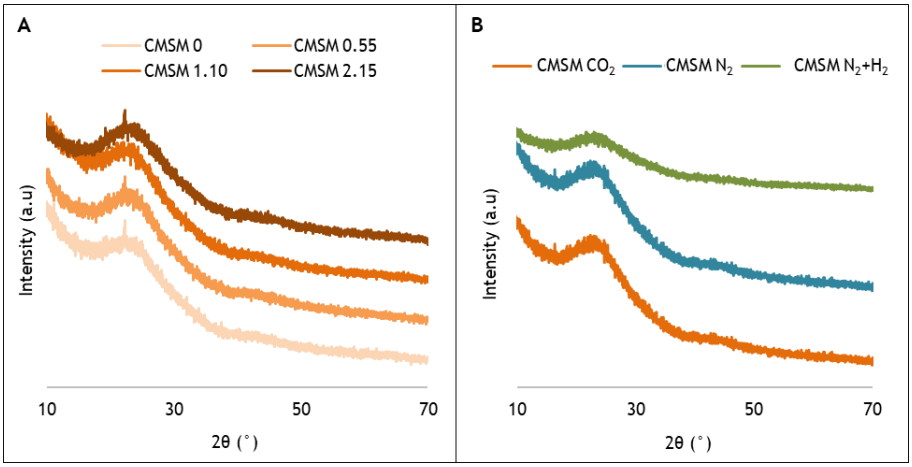


Figure 4.6. XRD analysis of the CMSMs produced with (**A**) different quantities of boehmite and (**B**) carbonized under different atmospheres.

Table 7. *d*-spacing values obtained with XRD analysis.

CMSM	Plane	2ϑ (°)	*d*-spacing (nm)
CMSM 0	(002)	23.87	0.372
CMSM 0.55	(002)	23.87	0.372
CMSM 1.10	(002)	23.34	0.381
CMSM 2.15	(002)	22.31	0.398
CMSM CO_2	(002)	23.34	0.381
CMSM N_2	(002)	23.14	0.384
CMSM N_2+H_2	(002)	23.26	0.382

In **Figure 4.6**, it is possible to define the plane (002), characteristic of the graphitic domains (sp^2 carbon). The boehmite peak, corresponding to the plane (200) should appear in the 2θ value in the range of 45-50°, however in this case the peaks are imperceptible. This can be because the carbon matrix is mainly non-crystalline forming a board peak. Additionally, the low boehmite content and well-dispersed nanoparticles further contribute to the limited sensitivity of the equipment, making it unable to detect these specific planes.

The distinction between the peaks of the different samples is not easily discernible in **Figure 4.6**. However, upon examining the *d*-spacing values associated with the (002) plane, it becomes apparent that there is a tendency for an increase as the boehmite content rises. It is important to notice that these results are not a measurement of the pore size of the CMSMs, however, the increase in *d*-spacing implies that the volume of the pores expands, indicating a corresponding increase in the permeability of the membranes. Regarding the carbonization atmospheres, the *d*-spacing values are very close to each other.

4.1.6 Raman spectroscopy

To understand how the carbon layers are distributed in the CMSM structure it was conducted a Raman spectroscopy test to each sample of carbon membrane. In **Figure 4.7** are presented the Raman spectra for the samples with different boehmite content and with different carbonization atmospheres. The peaks were deconvoluted into two Gaussian peaks using the ORIGIN software. The first peak, around 1,390 cm^{-1}, is recognized as the disorder band (D band) caused by structural defects and vibrational processes in the carbon lattice that break the symmetry. The second peak, around 1,590 cm^{-1}, is called the G band characteristic of the in plane stretching motion between sp^2 carbon atoms, representing the planar configuration sp^2 bounded carbon that constitutes graphene [71].

The ratio between the area of the two peaks is given in **Table 8**. Comparing the samples with different boehmite contents, carbonized in a CO_2 atmosphere, it is observed that the CMSM

1.10 exhibits the highest value of A_D/A_G. This reveals that the disorder of the carbon lattice increases up to this boehmite percentage. As the disorder increases, the free volume increases resulting in the formation of more micropores, that are responsible for higher permeabilities. In **Figure A.9** (see Appendix A) is possible to observe the difference of the carbon membrane surface in a sample with and without boehmite.

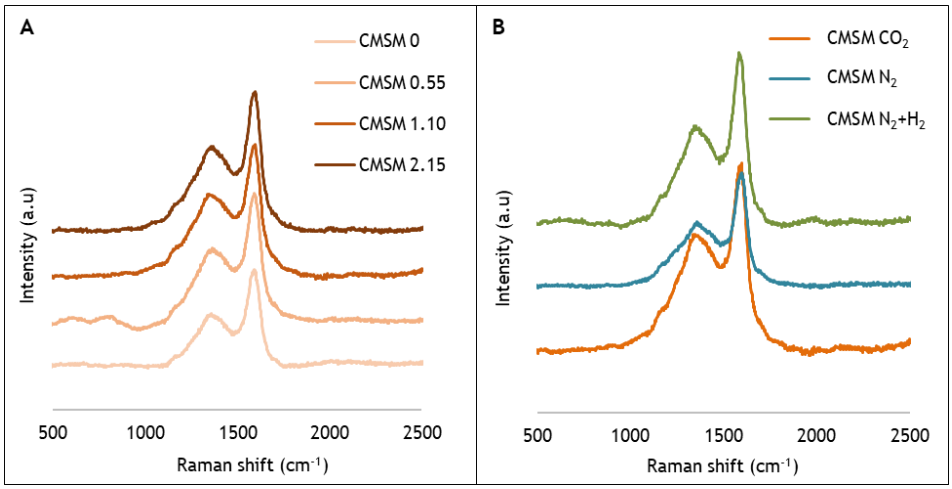


Figure 4.7. Raman spectra of the CMSMs produced with(**A**) different quantities of boehmite and (**B**) carbonized at different atmospheres.

When comparing the films with this same amount of boehmite but carbonized under different atmospheres, (**Figure 4.7B),** it can be concluded that a CO_2 atmosphere also increases the disorder of the carbon lattice. This finding is further demonstrated in the chapter dedicated to permeability tests.

Table 8. A_D/A_G values obtained by Raman technique.

CMSM	CMSM 0	CMSM 0.55	CMSM 1.10	CMSM 2.15	CMSM CO_2	CMSM N_2	CMSM $N_2 + H_2$
A_D/A_G	1.608	1.811	3.853	3.213	3.853	2.158	2.638

4.1.7 Water contact angle

Water contact angle measurements were made to determine the hydrophilicity of the produced carbon membranes. **Figure 4.8** presents the average water contact angle that was measured for the membranes with different boehmite content and carbonized under different atmospheres.

Looking at the results, all the carbon membranes present a water contact angle lower than 90 °, which means that the CMSM produced with cellulose as precursor are hydrophilic. The water contact angle progressively decreases as the boehmite content increases up to

1.10 wt. %. The optimum result of 61.2 ° is achieved with this concentration of boehmite. This indicates that boehmite enhances the hydrophilicity of the membranes that were produced for this work, but only up to a certain threshold below 2.15 wt. %. Regarding the carbonization atmosphere, an oxidative atmosphere showed to be favorable to the absorption of water and using an inert atmosphere the carbon membrane was shown to be less hydrophilic, which is attributed to the higher carbon content in its chemical structure, as seen previously with the EDS technique.

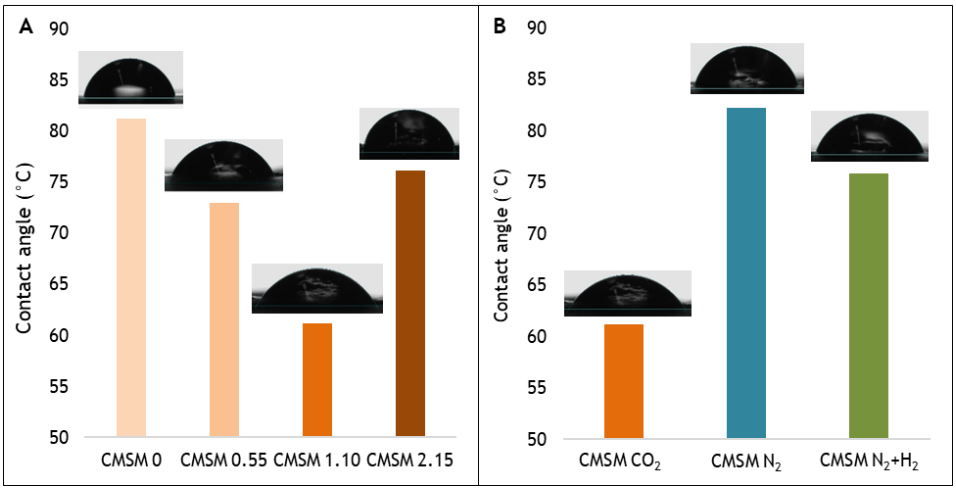


Figure 4.8. Water contact angle measurements of the CMSMs produced with (**A**) different quantities of boehmite and (**B**) carbonized under different atmospheres.

4.2 Permeation tests

The permeation tests of the several carbon membranes produced were carried out at 1 bar feed pressure and 25 °C, with gases of varying kinetic diameters, including hydrogen (0.289 nm), carbon dioxide (0.330 nm), oxygen (0.346 nm), and nitrogen (0.364 nm). In addition, the membrane's performance was evaluated when exposed to humidified nitrogen. The results can be separated in relation to boehmite content and carbonization atmosphere.

4.2.1 Boehmite content

Figure 4.9 represents both the results of single gas permeation as a function of the correspondent kinetic diameter and the selectivity of the membranes with different boehmite content and carbonized in a CO_2 atmosphere. It is important to mention that the membrane with 2.15 wt. % of boehmite content was not tested because it was not possible to glue it to the stainless-steel disc due to its fragility, and it broke on every attempt.

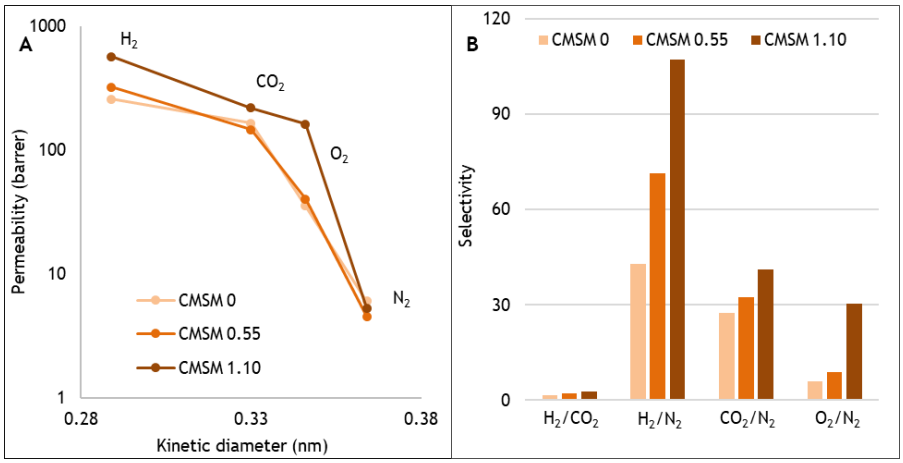


Figure 4.9. (**A**) Single gas permeabilities and (**B**) ideal selectivities of the CMSMs produced with different quantities of boehmite.

For every sample tested, the permeability of the membranes decreases as the kinetic diameter increases (**Figure 4.9A**), meaning that the molecular sieving mechanism is predominant in these membranes. By adding 0.55 wt. % of boehmite, the difference in permeability values is not very significant, but with 1.10 wt. % boehmite the permeability increased for all gases except for nitrogen. Focusing on **Figure 4.9B**, the selectivity of every pair of gases increased with boehmite content, specially the H_2/N_2 selectivity that increased from 43 without boehmite to 107 with 1.10 wt. % of boehmite. As both permeability and selectivity have increased suggests that the boehmite increased the volume of the micropores without impacting the ultramicroporous structure. The permeabilities and ideal selectivity results for each membrane tested are described in **Table A.3** and **Table A.4** (see Appendix A).

Table 9 shows the Robeson index for the H_2/N_2, O_2/N_2, H_2/CO_2 and CO_2/N_2 separations, calculated with Equation 8, and **Figure 4.10** the Robeson plots for the respective separations. Overall, H_2/N_2 and O_2/N_2 separation have shown the best results, being almost always above the Robeson upper bound. The Robeson index increases with the addition of boehmite, meaning that the boehmite nanoparticles enhance the performance of the CMSMs. These results are in line with the conclusions of the study by Poto *et al.* [50] and Araújo *et al.* [54].

Table 9. Robeson index of the CMSMs produced with different quantities of boehmite.

	Robeson Index			
	H_2/N_2	O_2/N_2	H_2/CO_2	CO_2/N_2
CMSM 0	0.78	0.91	0.45	0.41
CMSM 0.55	1.51	1.41	0.70	0.46
CMSM 1.10	3.33	6.13	1.06	0.68

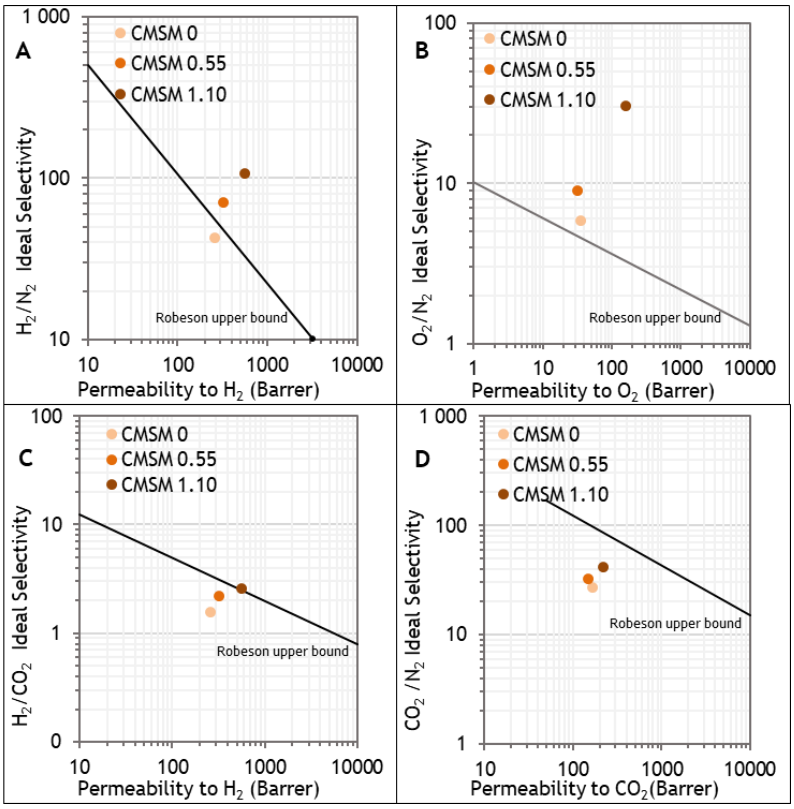


Figure 4.10. Robeson plots for the CMSMs produced with different quantities of boehmite for (**A**) H_2/N_2, (**B**) O_2/N_2, (**C**) H_2/CO_2 and (**D**) CO_2/N_2 separations.

In conclusion, regarding the boehmite content, the best membrane performance was achieved by the CMSM produced with 1.10 wt. % of boehmite, having the best results of both permeability and selectivity, as predicted by characterization tests such as Raman and XRD, which already showed an indication of better performance for this membrane. The permeability and selectivity in function of the *d*-spacing and the ratio of the area of the D and G peaks can be seen in **Figure 4.11.**

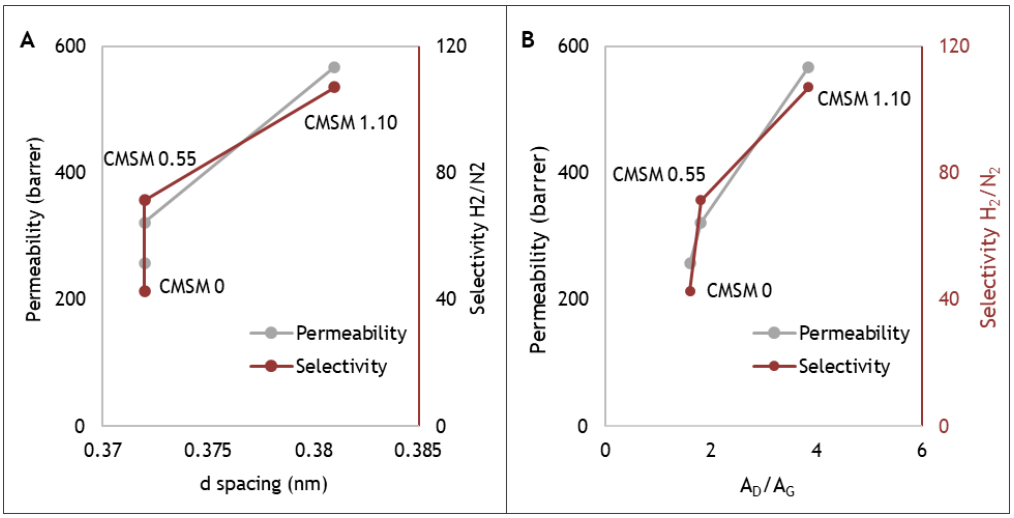


Figure 4.11. Permeability and selectivity in function of (**A**) the d-spacing and (**B**) A_D/A_G.

4.2.2 Carbonization atmosphere

The results of permeability and selectivity of the polymeric film with 1.10 wt. % of boehmite carbonized under different atmospheres are presented in **Figure 4.12**. Once again, it has been demonstrated that molecular sieving occurs in membranes of this type regardless of the type of atmosphere during the pyrolysis step, since the permeability decreases with increasing kinetic diameter. It is evident that an inert atmosphere yields the lowest permeability values while the addition of hydrogen to the nitrogen stream enhances permeability, making it more competitive to results obtained in an oxidizing atmosphere. In contrast, the selectivity of the CMSM produced in a reducing atmosphere was compromised (**Figure 4.12B**). Overall, the CO_2 atmosphere had the best results, both in permeability and selectivity. The permeabilities and ideal selectivity results for each membrane tested are described in **Table A.3** and **Table A.4** (see Appendix A).

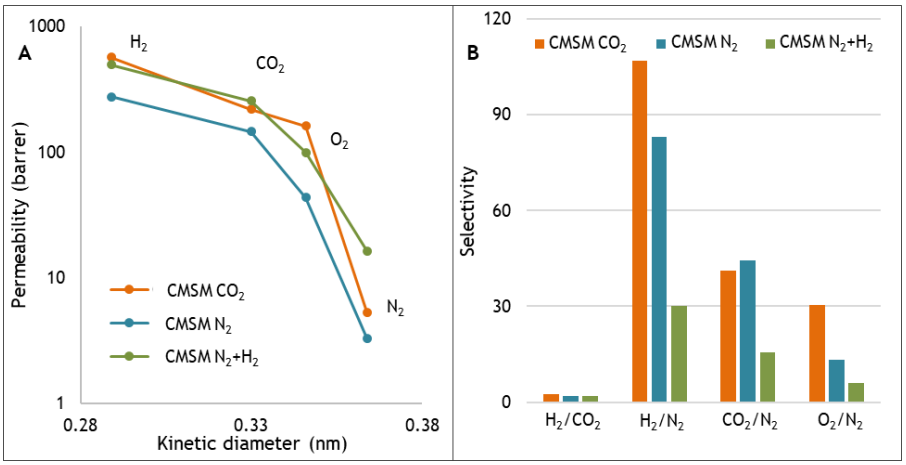


Figure 4.12. (**A**) Single gas permeabilities and (**B**) ideal selectivities of the CMSMs produced with different carbonization atmospheres.

Table 10 shows the Robeson index for the H_2/N_2, O_2/N_2, H_2/CO_2 and CO_2/N_2 separations, calculated with Equation 8 and **Figure 4.13** the Robeson plots for the respective separations. Overall, H_2/N_2 and O_2/N_2 separation have shown the best results for each carbonization atmosphere, being almost always above the Robeson upper bound.

Table 10. Robeson index of the CMSMs produced with different carbonization atmospheres.

	Robeson Index			
	H_2/N_2	O_2/N_2	H_2/CO_2	CO_2/N_2
CMSM CO_2	3.33	6.13	0.45	0.41
CMSM N_2	1.58	2.12	0.56	0.63
CMSM N_2+H_2	0.86	1.12	0.74	0.27

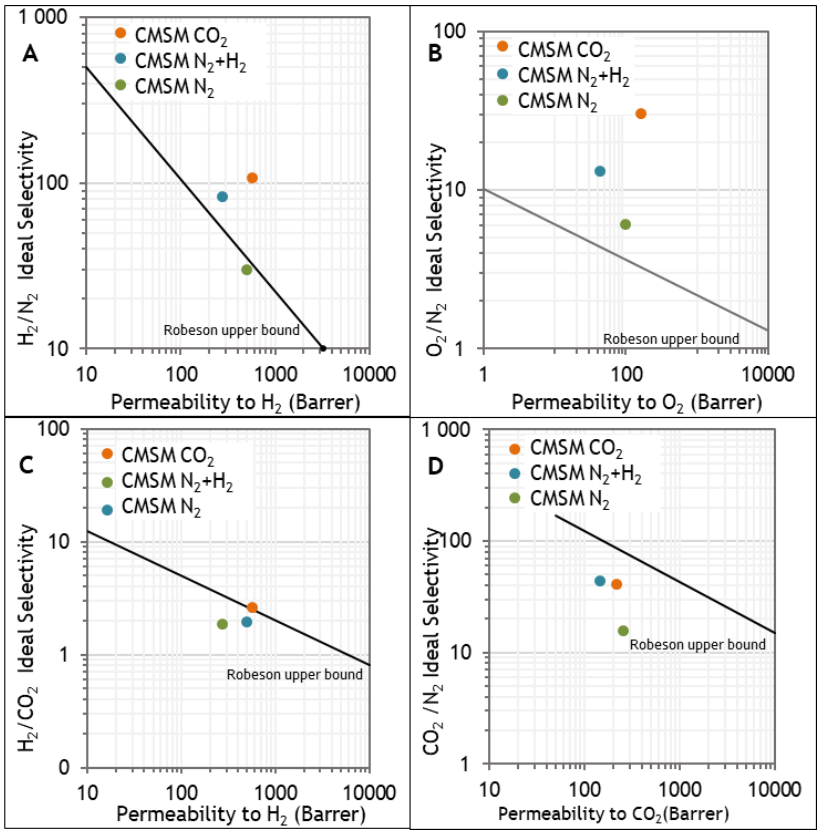


Figure 4.13. Robeson plots for the CMSMs produced with different carbonization atmospheres for (**A**) H_2/N_2, (**B**) O_2/N_2, (**C**) H_2/CO_2 and (**D**) CO_2/N_2 separations.

The trade-off between permeability and selectivity and better results for the CO_2 atmosphere can also be observed by relating the results of the permeation tests to the raman results, as shown in **Figure 4.14**.

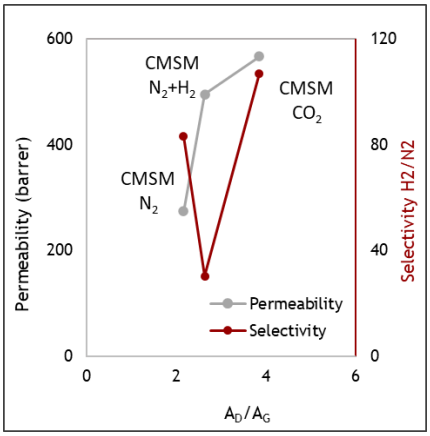


Figure 4.14. Permeability and selectivity in function of the A_D/A_G.

4.2.3 Humidified gas permeation experiments

In **Table 11** are presented the permeability values for humidified nitrogen compared to the permeability values for non-humidified nitrogen. In general, the permeability increased when the gas was humidified, meaning that the membranes produced with cellulose as precursor can

permeate water vapor molecules, as was reported by Rodrigues *et al*. [2]. Furthermore, the presence of boehmite nanoparticles favors the permeation of water molecules, since the permeability to nitrogen remains nearly constant across all CMSMs, while the permeability to humidified nitrogen increases. Regarding the carbonization atmospheres, although permeability is higher using an atmosphere containing nitrogen and hydrogen, the ratio between the humidified and non-humidified gas is lower. On the other hand, when an oxidizing atmosphere was used, the increase in permeability is much higher.

Table 11. Humidified gas permeability of the CMSMs produced with different quantities of boehmite and different carbonization atmospheres.

CMSM	Permeability (barrer)		
	N_2	N_2 hum	N_2 hum/N_2
CMSM 0	6	18	3
CMSM 0.55	5	23	5
CMSM 1.10	5	35	7
CMSM CO_2	5	35	7
CMSM N_2	3	7	2
CMSM N_2+H_2	16	25	2

These results serve as a strong indication of the permeation capacity of water molecules through the membranes that were produced, particularly the CMSM created using 1.10 wt. % of boehmite and carbonized in a CO_2 atmosphere. This conclusion corroborates the previous results observed in the contact angle measurements. This agrees with the lowest C/O ratio determined by EDS and the lowest water contact angle, which is the most hydrophilic membrane.

4.3 Water/solvent separation tests

4.3.1 Gas chromatography and permeation results

Following the previous results for the single gas permeation tests, the membrane with 1.10 wt. % of boehmite, carbonized with a CO_2 atmosphere, was chosen for the water/solvent separation tests.

The first attempt to carry out this type of tests was performed with the installation of **Figure A.4** (see Appendix A). The initial plan consisted in measuring the permeability of the membranes by determining the mass of permeate retained in the trap. The trials ran for 6 h, yet regardless of multiple attempts no permeate could be found in the trap. A study was then

performed to understand the reason of these results and the conclusion was that the area of the produced membranes was too small to reach any measurable content in the trap at the end of a reasonable test time. In comparison to the study carried out by Poto *et al.* [63], which utilized a similar installation and the same method to calculate the permeability, the area of their membranes was 150 times larger than the area of the CMSMs used in this dissertation work. Poto *et al.* [63] used carbon membranes, supported by a tubular alumina tube with a working area of approximately 30 cm^2, allowing them to collect the permeate after 40 min. In contrast, to achieve the same amount of permeate using the membranes of this dissertation it would be necessary to run the trial for 4 days.

To overcome this problem, a new approach was taken to the installation (**Figure 3.1**). The chromatogram of the direct injections of 1 ppm methanol and ethanol is illustrated in **Figure 4.15**. The first peak, at 2 min, corresponds to the set of all permanent gases present; at 2.4 min, the specific CO_2 peak appears and the last two peaks, at 8 and 8.3 min, are related to O_2 and N_2. The small peak observed at 4.8 min is associated with humidity, appearing by default in all tests, even when only grid gas is injected. However, it is an important result as it provides an indication where the water peak could come out. Both methanol and ethanol peaks are observed at 4.3 min, having the same retention time.

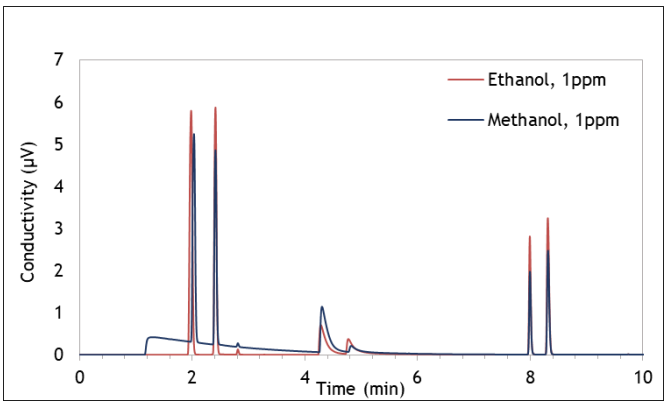


Figure 4.15. Chromatogram of the direct injections of methanol and ethanol.

The chromatograms of the separation of the water and methanol mixture with 50 vol. % of water, at 120 and 200 °C, are shown in **Figure 4.16.** The first peak is characteristic of nitrogen, that was the carrier gas utilized in the experiments. Comparing to **Figure 4.15**, methanol concentration must be well below 1 ppm, because no peak is seen at 4.3 min. In the other hand, a huge peak appeared in the zone of the water retention time, which means that, for both experiments, the permeate stream contained water and, interestingly the methanol concentration was below the detection limit of the GC.

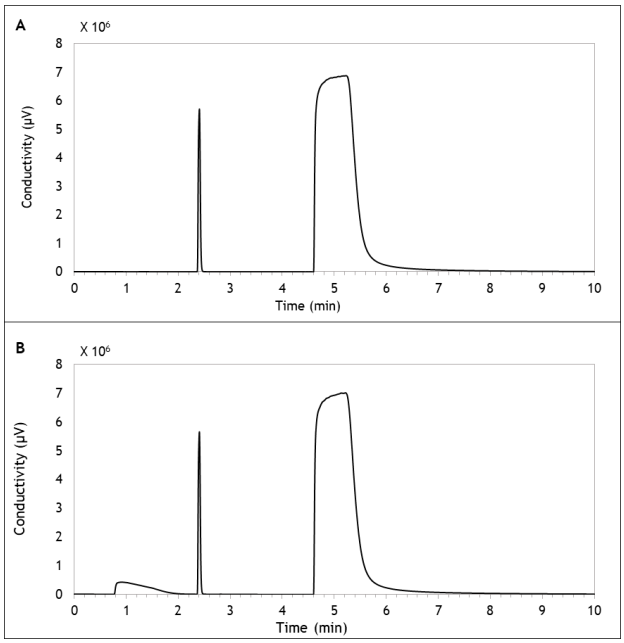


Figure 4.16. Chromatogram of the 50/50 vol. % methanol-water experiment at (**A**) 120 °C and (**B**) 200 °C.

Same conclusions were observed when carried out the experiment with a mixture of 70/30 vol. % of ethanol-water at 120 °C, as can be seen in **Figure 4.17**.

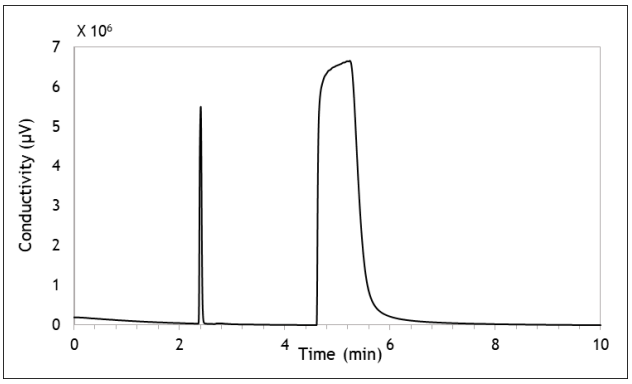


Figure 4.17. Chromatogram of the 70/30 vol. % ethanol-water experiment at 120 °C.

The permeance of water was then calculated with Equation 11 and the values for the three experiments are summarized in **Table 12**. Focusing on water/methanol separation, when increasing the temperature of the experiment, the permeance value increased. In water-ethanol trial, the composition of the feed is different, so it is not possible to compare the results with the other mixture. The results obtained agree with those in the literature, summarized in **Table 1** and **Table 2**. To evaluate the selectivity of the experiments, it was assumed that the carbon membrane permeated 1 ppm of methanol and ethanol. Based on this, the water/methanol selectivity was determined to be 10,618 at 120 °C and 12,260 at 200 °C, while water/ethanol selectivity at 120 °C was 6,691.

Table 12. Permeance results for the water/solvent separation experiments.

Feed (vol. %)	Feed Temperature (°C)	Permeance (mol·m^{-2}·h^{-1}·kPa^{-1})
50/50 water-methanol	120	0.435
50/50 water-methanol	200	0.502
30/70 water-ethanol	120	0.274

Whenever an experiment was carried out at 200 °C, the membrane stopped permeating after some time, no peaks were observed in the chromatograms and the values read with the dew point meter started to drop dramatically. Therefore, identical characterization tests, similar to the ones conducted prior to any separation experiment, were performed to comprehend the changes in the membrane.

4.3.2 Post experiments characterization tests

The SEM image (**Figure 4.18**) reveals unusual particles in the carbon membrane surface. The use of the EDS teqnique **(Figure 4.20A**) shows that new elements appeared in the chemical composition of the membrane, such as silicon, chlorine, sulfur and calcium. This finding is also supported by the FTIR spectrum shown in **Figure 4.19**, where a comparison with the membrane prior to exposure to organic solvents or high temperatures indicates the appearance of new bands within the range of 1,050 to 700 cm^{-1}.These bands are caracteristic of Si-C, C-Cl and Si-O-Si stretching vibrations as well as rocking vibrations between silicon and the methyl group. This appearance of new compounds may be related with the decomposition of the glue used to glue the membranes to the stainless-steel disk or the decomposition of the silicone O-rings.

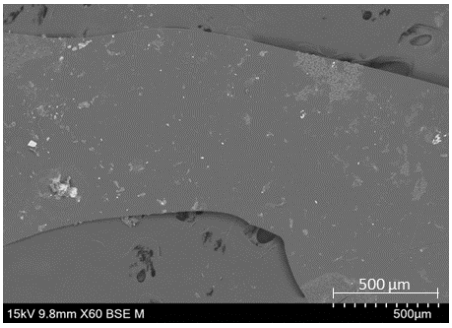
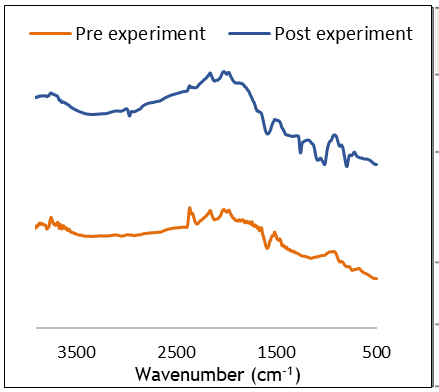


Figure 4.18. SEM image for the CMSM 1.10 post experiment.



Wavenumber (cm^{-1})	Functional group	Assignment
1029	Si-O-Si in siloxanes	Si-O-Si antisymmetric stretch
871	Si-C in organosilicon compounds	Si-C stretch
840	Si-CH3 in silanes	Si-CH3 rocking
738	C-Cl alkyl chlorides	C-Cl stretch

Figure 4.19. FTIR spectra of CMSM 1.10 pre and post experiment and new bands assignments.

The carbon membrane became hydrophobic after the experiment, since the water contact angle increased to more than 90 ° as illustrated in **Figure 4.20B**, which is an important result, being in agreement with the fact that the membrane no longer permeates.

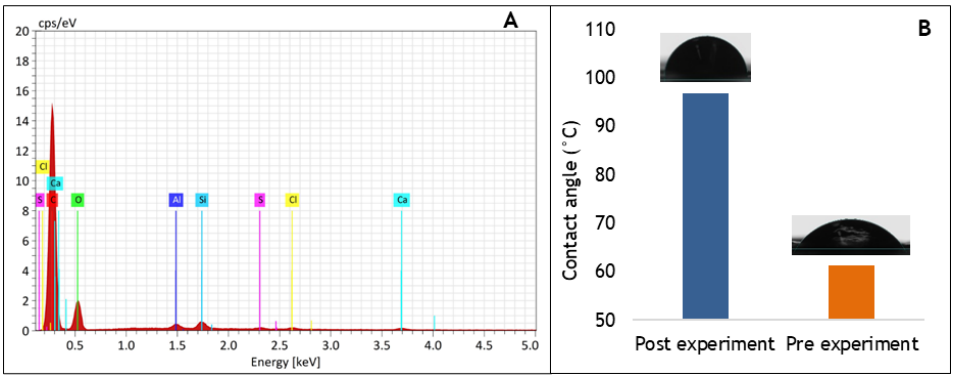


Figure 4.20. (**A**) EDS spectrum and (**B**) water contact angle measurements for the CMSM 1.10 pre and post experiment.

Comparing Raman microscopy and XRD analysis, **Figure A.10** (see Appendix A), before and after the trials, the ratio A_D/A_G decreased from 3.85 to 1.90 and the d-spacing increased from 0.381 nm to 0.394 nm, respectively. The FTIR and EDS technique reveal the emergence of new functional groups, which could potentially have originated from the glue or the O-rings. The Raman spectroscopy might be detecting these areas where particles of these substances are present, rather than the crystalline structure of the material.

5 Conclusion

Unsupported cellulose-based CMSMs with boehmite nanoparticles were successfully prepared, characterized and tested.

SEM images showed that the structure of the polymeric film became more asymmetric after the incorporation of boehmite nanoparticles. However, the carbonization step led to the collapse of the pores, resulting again in a denser structure. TGA test indicated that the addition of boehmite nanoparticles enhanced the membrane stability, increasing the temperature at which the polymer experienced maximum degradation. In terms of chemical composition, EDS technique showed that the C/O and C/Al ratios decreased as the boehmite content increased, as expected. Moreover, in terms of carbonization atmosphere, CMSM prepared under an inert atmosphere revealed a higher carbon content. These results were in agreement with water contact angle measurements, which showed that membranes with lower carbon content exhibited increased hydrophilicity. FTIR spectra revealed that, in general, the OH band was less intensive after carbonization and higher boehmite concentration also contributed to a reduction in this band's intensity. Similar observations were made for N≡C stretching vibrations and substituted benzene rings bonds. Different carbonization atmospheres demonstrated differences in C-O-C stretching vibrations band, that was more intense with an oxidative atmosphere. The carbon membrane with 1.10 wt. % of boehmite and the oxidizing atmosphere indicated to have more free volume, meaning more micropores as was possible to conclude by XRD and Raman spectroscopy.

Based on the results of single gas permeation tests, it can be concluded that boehmite significantly improved both permeability and selectivity. Permeability duplicated, except for N_2, with the addiction of 1.10 wt. % of boehmite, while selectivity increased for every pair of gases, specially H_2/N_2 selectivity, that increased from 43 to 107. These conclusions were supported by the Robeson Index, which showed that the CMSM 1.10 surpassed the Robeson upper bound for almost all the separations. Among the different carbonization atmospheres studied, the inert atmosphere resulted in the CMSM with the lowest permeability values, whereas both reducing and oxidizing atmospheres yielded CMSM with roughly doubled permeability. In contrast, the CMSM prepared under reducing atmosphere exhibited lower selectivities compared to the CMSM prepared under the two other atmospheres, with the oxidizing atmosphere being the best option as confirmed by the Robeson index. Furthermore, all the membranes demonstrated an increase permeability to humidified gas showing that the cellulose-based carbon membranes produced for this work had hydrophilic properties. The best performance was obtained with the carbon membrane with 1.10 wt. % of boehmite, carbonized with an atmosphere of CO_2.

The proof of concept of water/solvent separation tests was successfully accomplished. A dedicated installation was constructed to test different solvents, namely methanol and ethanol. The chromatograms constantly showed the presence of water in the permeate stream in every experiment. The obtained permeance value were 0.435 and 0.502 $mol \cdot m^{-2} \cdot h^{-1} \cdot kPa^{-1}$ for the mixture with 50 vol. % of methanol at 120 and 200 °C, respectively, which indicated that higher temperatures enhance permeability. For the mixture with 70 vol. % of ethanol at 120 °C it was obtained a permeance of 0.274 $mol \cdot m^{-2} \cdot h^{-1} \cdot kPa^{-1}$. These results provide supporting evidence for the successful separation of water and organic solvents using the developed membrane system.

Following the experiments conducted at 200 °C, the membrane stopped permeating indicating structural transformations. FTIR and EDS characterization tests detected new vibrations and compounds, namely silicon, chloride, calcium and sulfur that can be caused by degradation of the glue or the O-rings. Water contact measurements revealed that the carbon membrane became hydrophobic and with Raman spectroscopy it was seen that the disorder of the carbon plans decreased.

6 Assessment of the work done

6.1 Objectives Achieved

The first objective of this dissertation was to understand the membrane separation processes and to prepare hydrophilic carbon molecular sieve membranes, which was successfully accomplished. Then, the prepared membranes were chemically and morphologically characterized, as proposed. To test the performance of the membranes in terms of permeability and selectivity, the objective was to carry out single gas permeation tests and the proof of concept for water/solvent separation tests, which were both successfully completed. This study also fulfilled the company's proposed goal of studying more efficient and sustainable alternatives to purify methanol.

6.2 Other Work Carried Out

During the last weeks, knowledge regarding the procedure for producing carbon membranes supported in ceramic tubes started to be acquired.

6.3 Limitations and Future Work

The facility used for this dissertation work was an incorporation of existing equipment in the lab. This arrangement served the purpose of conducting a proof of concept for the study and gaining insights into the fundamental equipment required for a future installation, designed specifically for the vapor separation tests. Thus, an installation is suggested, in **Figure 6.1**, that could be implemented in forthcoming tests. To guarantee that the feed mixture is in vapor phase when it arrives to the membrane cell, it can be utilized a Controlled Evaporation and Mixing (CEM). Mass flow controllers, pressure and dew point meters should be implemented in every stream (feed, retentate and permeate) and it is necessary that the line arriving at the CG is heated to prevent any risk of condensation.

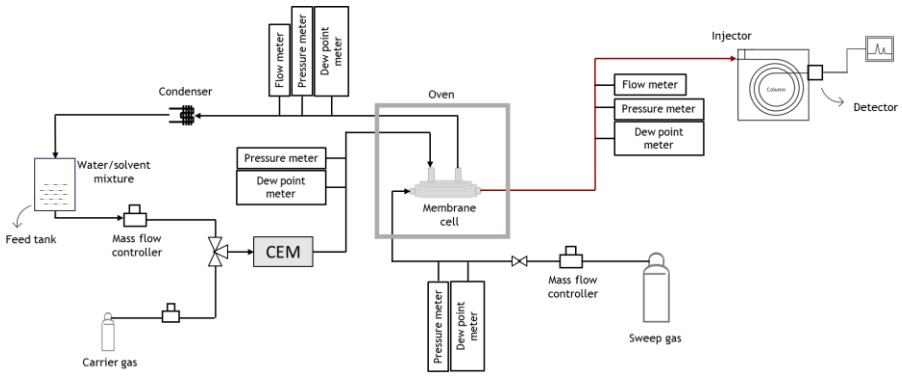


Figure 6.1. Suggestion of future setup for water/solvent separation tests.

For future work, it is important to characterize the microporous structure of the membranes by determining CO_2 adsorption isotherms (since CO_2 is smaller than N_2) and applying Dubinin-Radushkevich equation to determine the micropore volume and pore size distribution. In order to solve the problem of the membrane no longer permeating, it is imperative to explore alternative glues and utilize different O-rings. Given the limited area of the current membranes employed in this process, it will be crucial to develop tubular supported membranes that offer a significantly larger working area.

6.4 Final Assessment

I found the work proposed extremely interesting and challenging due to the technology addressed being very new. When I started this project, the state of the art for the separation of water/solvent mixtures was only about pervaporation, being vapor gas separation a new technology that has been very little explored so far. Having completed my dissertation, I am strongly convinced that the membrane technology I studied presents a promising approach for alcohol dehydration. While there is still ongoing research on supported membranes, I believe that they represent the next advancement needed for the practical implementation of this technology in the industry.

In addition to gaining a lot of theoretical knowledge about membrane technology, my work was very practical, having learned about various topics and how to use several equipments. These months tested my critical thinking skills and, above all, my resilience and determination to overcome all the obstacles that occurred.

Although I dedicated a significant amount of time to laboratory work, the experience of conducting my research in a business environment proved to be highly rewarding. It gave me the opportunity to fully comprehend the practical implications of my work and granted me valuable insights into renewable energy projects within a corporate context.

7 References

[1] U. N. C. Actions. "For a livable climate: Net-zero commitments must be backed by credible action." https://www.un.org/en/climatechange/net-zero-coalition (accessed 02/16, 2023).

[2] S. C. Rodrigues, M. Andrade, J. Moffat, F. D. Magalhães, and A. Mendes, "Preparation of carbon molecular sieve membranes from an optimized ionic liquid-regenerated cellulose precursor," *Journal of Membrane Science*, vol. 572, pp. 390-400, 2019/02/15/ 2019, doi: https://doi.org/10.1016/j.memsci.2018.11.027.

[3] IEA. "Global energy-related CO2 emissions by sector." IEA. https://www.iea.org/data-and-statistics/charts/global-energy-related-co2-emissions-by-sector (accessed 02/16, 2023).

[4] M. R. a. P. R. Hannah Ritchie. "CO_2 and Greenhouse Gas Emissions." OurWorldInData.org. https://ourworldindata.org/co2-and-greenhouse-gas-emissions (accessed 02/16, 2023).

[5] H. Ritchie. "Cars, planes, trains: where do CO2 emissions from transport come from?" OurWorldinData.org. https://ourworldindata.org/co2-emissions-from-transport (accessed 02/16, 2023).

[6] C. F. Chia-wen Carmen Hsieh. "Biofuels for the marine shipping sector: An overview and analysis of sector infrastructure, fuel technologies and regulations." IEA Bioenergy. https://www.ieabioenergy.com/wp-content/uploads/2018/02/Marine-biofuel-report-final-Oct-2017.pdf (accessed 02/17, 2023).

[7] ENGIE. "E-fuels, what are they?" ENGIE. https://www.engie.com/en/news/e-fuels-what-are-they (accessed 02/17, 2023).

[8] M. I. IRENA, "Innovation Outlook : Renewable Methanol, International Renewable Energy Agency," 2021. [Online]. Available: https://www.irena.org/publications/2021/Jan/Innovation-Outlook-Renewable-Methanol

[9] M. INSTITUTE. "RENEWABLE METHANOL." METHANOL INSTITUTE. https://www.methanol.org/renewable/ (accessed 02/17, 2023).

[10] M. INSTITUTE. "APPLICATIONS." METHANOL INSTITUTE. https://www.methanol.org/applications/ (accessed 02/17, 2023).

[11] H. Nieminen, A. Laari, and T. Koiranen, "CO2 Hydrogenation to Methanol by a Liquid-Phase Process with Alcoholic Solvents: A Techno-Economic Analysis," *Processes*, vol. 7, no. 7, 2019, doi: 10.3390/pr7070405.

[12] Winarto, D. Takaiwa, E. Yamamoto, and K. Yasuoka, "Water-methanol separation with carbon nanotubes and electric fields," *Nanoscale*, vol. 7, no. 29, pp. 12659-65, Aug 7 2015, doi: 10.1039/c5nr02182k.

[13] C. Y. Chuah, "Membranes for Gas Separation and Purification Processes," *Membranes (Basel)*, vol. 12, no. 6, Jun 15 2022, doi: 10.3390/membranes12060622.

[14] P. H. T. Ngamou, M. E. Ivanova, O. Guillon, and W. A. Meulenberg, "High-performance carbon molecular sieve membranes for hydrogen purification and pervaporation dehydration of organic solvents," *Journal of Materials Chemistry A*, vol. 7, no. 12, pp. 7082-7091, 2019, doi: 10.1039/c8ta09504c.

[15] G. Bernardo, T. Araújo, T. da Silva Lopes, J. Sousa, and A. Mendes, "Recent advances in membrane technologies for hydrogen purification," *International Journal of Hydrogen Energy*, vol. 45, no. 12, pp. 7313-7338, 2020, doi: 10.1016/j.ijhydene.2019.06.162.

[16] P. Greene. "Basics Of Biogas Upgrading." BioCycle. https://www.biocycle.net/basics-biogas-upgrading/ (accessed 03/21, 2023).

[17] G. C. Paola Bernardo, "30 Years of Membrane Technology for Gas Separation," *Chemical Engineering Transactions* 2013, doi: 10.3303/CET1332334.

[18] A. Kayvani Fard, G. McKay, A. Buekenhoudt, H. Al Sulaiti, F. Motmans, M. Khraisheh, and M. Atieh, "Inorganic Membranes: Preparation and Application for Water Treatment and Desalination," (in eng), *Materials (Basel)*, vol. 11, no. 1, Jan 5 2018, doi: 10.3390/ma11010074.

[19] Marketsandmarkets, "Gas Separation Membranes Market by Material type (Polyimide & Polyaramide, Polysulfone, and Cellulose Acetate), Application (Nitrogen Generation & Oxygen Enrichment, Carbon Dioxide Removal, Vapor/Gas separation, Vapor/Vapor Separation, AD),Module (SW,HF) and Region - Global Forecast to 2026," 2022. [Online]. Available: https://www.marketsandmarkets.com/Market-Reports/gas-separation-membrane-market-50564392.html

[20] M. Mulder, *Basic Principles of Membrane Technology*, 2 ed. Springer Dordrecht, 1996, p. 564.

[21] X. Li and J. Li, "Fluxes and Driving Forces in Membrane Separation Processes," in *Encyclopedia of Membranes*, E. Drioli and L. Giorno Eds. Berlin, Heidelberg: Springer Berlin Heidelberg, 2015, pp. 1-3.

[22] T. O. M. Database. "Introduction to membrane science." https://openmembranedatabase.org/membrane-science/ (accessed 02/20, 2023).

[23] K. S. W. Sing, "Reporting physisorption data for gas/solid systems with special reference to the determination of surface area and porosity (Recommendations 1984)," *Pure and Applied Chemistry*, vol. 57, no. 4, pp. 603-619, 1985, doi: doi:10.1351/pac198557040603.

[24] M. Yoshimune and K. Haraya, "ASYMMETRIC CARBON MOLECULAR SIEVE MEMBRANES BASED ON POLY (PHENYLENE OXIDE) FOR GAS SEPARATION," 2006.

[25] S. Sonawane, P. Thakur, S. H. Sonawane, and B. A. Bhanvase, "Chapter 17 - Nanomaterials for membrane synthesis: Introduction, mechanism, and challenges for wastewater treatment," in *Handbook of Nanomaterials for Wastewater Treatment*, B. Bhanvase, S. Sonawane, V. Pawade, and A. Pandit Eds.: Elsevier, 2021, pp. 537-553.

[26] P. S. Tin, H. Y. Lin, R. C. Ong, and T.-S. Chung, "Carbon molecular sieve membranes for biofuel separation," *Carbon*, vol. 49, no. 2, pp. 369-375, 2011/02/01/ 2011, doi: https://doi.org/10.1016/j.carbon.2010.09.031.

[27] L. M. Robeson, "The upper bound revisited," *Journal of Membrane Science*, vol. 320, no. 1, pp. 390-400, 2008/07/15/ 2008, doi: https://doi.org/10.1016/j.memsci.2008.04.030.

[28] Marketsandmarkets. "Membranes Market by Material(Polymeric, ceramic), Technology (RO, MF, UF, NF), Applications (Water& Wastewater Treatment, Industrial Processing), & Region (North America, Europe, APAC, Middle East & Africa, South America) - Global Forecast to 2027." Marketsandmarkets. https://www.marketsandmarkets.com/Market-Reports/membranes-market-1176.html?gclid=Cj0KCQjwlPWgBhDHARIsAH2xdNeNbE-AJvnC45un0RUldYQbqAUZib_DJ4CVwyrAfCzQMKuqia5DSdYaAnbsEALw_wcB (accessed 02/17, 2023).

[29] W. N. W. Salleh, A. F. Ismail, T. Matsuura, and M. S. Abdullah, "Precursor Selection and Process Conditions in the Preparation of Carbon Membrane for Gas Separation: A

Review," *Separation & Purification Reviews,* vol. 40, no. 4, pp. 261-311, 2011/04/18 2011, doi: 10.1080/15422119.2011.555648.

[30] R. D. Noble, "Perspectives on mixed matrix membranes," *Journal of Membrane Science,* vol. 378, no. 1, pp. 393-397, 2011/08/15/ 2011, doi: https://doi.org/10.1016/j.memsci.2011.05.031.

[31] P. Pandey and R. S. Chauhan, "Membranes for gas separation," *Progress in Polymer Science,* vol. 26, no. 6, pp. 853-893, 2001/08/01/ 2001, doi: https://doi.org/10.1016/S0079-6700(01)00009-0.

[32] S. A. Reinecke and B. E. Sleep, "Knudsen diffusion, gas permeability, and water content in an unconsolidated porous medium," *Water Resources Research,* vol. 38, no. 12, pp. 16-1-16-15, 2002, doi: https://doi.org/10.1029/2002WR001278.

[33] M. B. Karimi, S. Hassanajili, and G. Khanbabaei, "Capillary condensation mechanism for gas transport in fiber reinforced poly (ether-b-amide) membranes," *Chemical Engineering Research and Design,* vol. 148, pp. 180-190, 2019/08/01/ 2019, doi: https://doi.org/10.1016/j.cherd.2019.06.002.

[34] M. J. Vaezi, M. E. Kojabad, M. M. Beiragh, and A. A. Babaluo, "Chapter 8 - Transport Mechanism and Modeling of Microporous Zeolite Membranes," in *Current Trends and Future Developments on (Bio-) Membranes*, A. Basile and K. Ghasemzadeh Eds.: Elsevier, 2019, pp. 185-203.

[35] A. F. Ismail and L. I. B. David, "A review on the latest development of carbon membranes for gas separation," *Journal of Membrane Science,* vol. 193, no. 1, pp. 1-18, 2001/10/31/ 2001, doi: https://doi.org/10.1016/S0376-7388(01)00510-5.

[36] F. Pişkin, "A Combinatorial Study on Hydrogen Separation Membranes," 2018.

[37] A. Amira, D. Huu, L. Ali, and C. Chil-Hung, "Mass Transfer Mechanisms and Transport Resistances in Membrane Separation Process," in *Mass Transfer*, S. Marek Ed. Rijeka: IntechOpen, 2015, p. Ch. 2.

[38] L. Chemistry. "Henry's Law." LibreTexts Chemistry. https://chem.libretexts.org/Bookshelves/Physical_and_Theoretical_Chemistry_Textbook_Maps/Supplemental_Modules_(Physical_and_Theoretical_Chemistry)/Physical_Properties_of_Matter/Solutions_and_Mixtures/Ideal_Solutions/Dissolving_Gases_In_Liquids%2C_Henry's_Law (accessed 03/02, 2023).

[39] Y. H. Yoon and R. P. Lively, "Co-transport of water and p-xylene through carbon molecular sieve membranes," *Journal of Membrane Science,* vol. 654, p. 120495, 2022/07/15/ 2022, doi: https://doi.org/10.1016/j.memsci.2022.120495.

[40] K. Friess, P. Izák, M. Kárászová, M. Pasichnyk, M. Lanč, D. Nikolaeva, P. Luis, and J. C. Jansen, "A Review on Ionic Liquid Gas Separation Membranes," *Membranes,* vol. 11, no. 2, p. 97, 2021. [Online]. Available: https://www.mdpi.com/2077-0375/11/2/97.

[41] J. C. Jansen, "Ideal Gas Selectivity," in *Encyclopedia of Membranes*, E. Drioli and L. Giorno Eds. Berlin, Heidelberg: Springer Berlin Heidelberg, 2016, pp. 1-1.

[42] T. Araujo, G. Bernardo, and A. Mendes, "Cellulose-Based Carbon Molecular Sieve Membranes for Gas Separation: A Review," *Molecules,* vol. 25, no. 15, Aug 1 2020, doi: 10.3390/molecules25153532.

[43] H. Richter, H. Voss, N. Kaltenborn, S. Kamnitz, A. Wollbrink, A. Feldhoff, J. Caro, S. Roitsch, and I. Voigt, "High-Flux Carbon Molecular Sieve Membranes for Gas Separation," *Angew Chem Int Ed Engl,* vol. 56, no. 27, pp. 7760-7763, Jun 26 2017, doi: 10.1002/anie.201701851.

[44] M. Kiyono, P. J. Williams, and W. J. Koros, "Effect of pyrolysis atmosphere on separation performance of carbon molecular sieve membranes," *Journal of Membrane Science,* vol.

359, no. 1, pp. 2-10, 2010/09/01/ 2010, doi: https://doi.org/10.1016/j.memsci.2009.10.019.

[45] O. Sanyal, C. Zhang, G. B. Wenz, S. Fu, N. Bhuwania, L. Xu, M. Rungta, and W. J. Koros, "Next generation membranes —using tailored carbon," *Carbon,* vol. 127, pp. 688-698, 2018/02/01/ 2018, doi: https://doi.org/10.1016/j.carbon.2017.11.031.

[46] S. Lagorsse, F. D. Magalhães, and A. Mendes, "Aging study of carbon molecular sieve membranes," *Journal of Membrane Science,* vol. 310, no. 1, pp. 494-502, 2008/03/05/ 2008, doi: https://doi.org/10.1016/j.memsci.2007.11.025.

[47] T. Araújo, M. Andrade, G. Bernardo, and A. Mendes, "Stable cellulose-based carbon molecular sieve membranes with very high selectivities," *Journal of Membrane Science,* vol. 641, p. 119852, 2022/01/01/ 2022, doi: https://doi.org/10.1016/j.memsci.2021.119852.

[48] J. E. Koresh and A. Sofer, "Molecular Sieve Carbon Permselective Membrane. Part I. Presentation of a New Device for Gas Mixture Separation," *Separation Science and Technology,* vol. 18, no. 8, pp. 723-734, 1983/06/01 1983, doi: 10.1080/01496398308068576.

[49] S. J. Kim, Y. Kwon, D. Kim, H. Park, Y. H. Cho, S. E. Nam, and Y. I. Park, "A Review on Polymer Precursors of Carbon Molecular Sieve Membranes for Olefin/Paraffin Separation," (in eng), *Membranes (Basel),* vol. 11, no. 7, Jun 29 2021, doi: 10.3390/membranes11070482.

[50] S. Poto, J. G. H. Endepoel, M. A. Llosa-Tanco, D. A. Pacheco-Tanaka, F. Gallucci, and M. F. Neira d'Angelo, "Vapor/gas separation through carbon molecular sieve membranes: Experimental and theoretical investigation," *International Journal of Hydrogen Energy,* vol. 47, no. 21, pp. 11385-11401, 2022/03/08/ 2022, doi: https://doi.org/10.1016/j.ijhydene.2021.10.155.

[51] A. B. Fuertes, D. M. Nevskaia, and T. A. Centeno, "Carbon composite membranes from Matrimid® and Kapton® polyimides for gas separation," *Microporous and Mesoporous Materials,* vol. 33, no. 1, pp. 115-125, 1999/12/15/ 1999, doi: https://doi.org/10.1016/S1387-1811(99)00129-8.

[52] P. S. Tin, T.-S. Chung, and A. J. Hill, "Advanced Fabrication of Carbon Molecular Sieve Membranes by Nonsolvent Pretreatment of Precursor Polymers," *Industrial & Engineering Chemistry Research,* vol. 43, no. 20, pp. 6476-6483, 2004/09/01 2004, doi: 10.1021/ie049606c.

[53] A. C. f. life. "Cellulose." ACS Chemistry for life. https://www.acs.org/molecule-of-the-week/archive/c/cellulose.html (accessed 03/07, 2023).

[54] F. B. Tiago Araújo, José M. Sousa, Gabriel Bernardo and and A. Mendes, "Preparation and Characterization of Free-Standing Composite Cellulose-Based Carbon Molecular Sieve Membranes," *International Journal of Membrane Science and Technology,* 2022, doi: 10.15379/2410-1869.2022.11.

[55] Y. K. Ong, H. Wang, and T.-S. Chung, "A prospective study on the application of thermally rearranged acetate-containing polyimide membranes in dehydration of biofuels via pervaporation," *Chemical Engineering Science,* vol. 79, pp. 41-53, 2012/09/10/ 2012, doi: https://doi.org/10.1016/j.ces.2012.05.013.

[56] Y. M. Xu, Y. P. Tang, T.-S. Chung, M. Weber, and C. Maletzko, "Polyarylether membranes for dehydration of ethanol and methanol via pervaporation," *Separation and Purification Technology,* vol. 193, pp. 165-174, 2018/03/20/ 2018, doi: https://doi.org/10.1016/j.seppur.2017.11.004.

[57] S. Sommer and T. Melin, "Performance evaluation of microporous inorganic membranes in the dehydration of industrial solvents," *Chemical Engineering and Processing: Process*

Intensification, vol. 44, no. 10, pp. 1138-1156, 2005/10/01/ 2005, doi: https://doi.org/10.1016/j.cep.2005.02.006.

[58] J. Zhang and W. Liu, "Thin porous metal sheet-supported NaA zeolite membrane for water/ethanol separation," *Journal of Membrane Science,* vol. 371, no. 1, pp. 197-210, 2011/04/01/ 2011, doi: https://doi.org/10.1016/j.memsci.2011.01.032.

[59] K. Ueno, H. Negishi, T. Okuno, T. Saito, H. Tawarayama, S. Ishikawa, M. Miyamoto, S. Uemiya, Y. Sawada, and Y. Oumi, "A simple secondary growth method for the preparation of silicalite-1 membrane on a tubular silica support via gel-free steam-assisted conversion," *Journal of Membrane Science,* vol. 542, pp. 150-158, 2017/11/15/ 2017, doi: https://doi.org/10.1016/j.memsci.2017.08.005.

[60] L. Peng, Z. Wu, B. Wang, H. Liu, C. Zhang, and X. Gu, "Fabrication of high-stability W-MFI zeolite membranes for ethanol/water mixture separation," *Journal of Membrane Science,* vol. 659, p. 120729, 2022/10/05/ 2022, doi: https://doi.org/10.1016/j.memsci.2022.120729.

[61] A. Rahimalimamaghani, D. A. Pacheco Tanaka, M. A. Llosa Tanco, F. Neira D'Angelo, and F. Gallucci, "New hydrophilic carbon molecular sieve membranes for bioethanol dehydration via pervaporation," *Chemical Engineering Journal,* vol. 435, p. 134891, 2022/05/01/ 2022, doi: https://doi.org/10.1016/j.cej.2022.134891.

[62] W. Zhang, G. Li, Y. Fang, and X. Wang, "Maleic anhydride surface-modification of crosslinked chitosan membrane and its pervaporation performance," *Journal of Membrane Science,* vol. 295, no. 1, pp. 130-138, 2007/05/31/ 2007, doi: https://doi.org/10.1016/j.memsci.2007.03.001.

[63] S. Poto, A. Aguirre, F. Huigh, M. A. Llosa-Tanco, D. A. Pacheco-Tanaka, F. Gallucci, and M. F. Neira d'Angelo, "Carbon molecular sieve membranes for water separation in CO2 hydrogenation reactions: Effect of the carbonization temperature," *Journal of Membrane Science,* vol. 677, p. 121613, 2023/07/05/ 2023, doi: https://doi.org/10.1016/j.memsci.2023.121613.

[64] P. B. Raja, K. R. Munusamy, V. Perumal, and M. N. M. Ibrahim, "5 - Characterization of nanomaterial used in nanobioremediation," in *Nano-Bioremediation : Fundamentals and Applications*, H. M. N. Iqbal, M. Bilal, and T. A. Nguyen Eds.: Elsevier, 2022, pp. 57-83.

[65] R. J. Narayan, "28.8 Fourier Transform Infrared Spectroscopy," in *ASM Handbook, Volume 23 - Materials for Medical Devices*: ASM International.

[66] C. metrology. "Water Contact Angle (WCA)." https://covalentmetrology.com/techniques/water-contact-angle-wca/ (accessed 2023).

[67] S. J. Metz, W. J. C. van de Ven, J. Potreck, M. H. V. Mulder, and M. Wessling, "Transport of water vapor and inert gas mixtures through highly selective and highly permeable polymer membranes," *Journal of Membrane Science*, vol. 251, no. 1, pp. 29-41, 2005/04/01/ 2005, doi: https://doi.org/10.1016/j.memsci.2004.08.036.

[68] B. E. Poling, J. M. Prausnitz, and J. P. O'Connell, *Properties of Gases and Liquids*, 5th Edition ed. New York: McGraw-Hill Education (in en), 2001.

[69] C. Araujo-Andrade, F. Ruiz, J. R. Martínez-Mendoza, and H. Terrones, "Infrared and Raman spectra, conformational stability, ab initio calculations of structure, and vibrational assignment of α and β glucose," *Journal of Molecular Structure: THEOCHEM,* vol. 714, no. 2, pp. 143-146, 2005/02/14/ 2005, doi: https://doi.org/10.1016/j.theochem.2004.09.041.

[70] K. A. Trick and T. E. Saliba, "Mechanisms of the pyrolysis of phenolic resin in a carbon/phenolic composite," *Carbon,* vol. 33, no. 11, pp. 1509-1515, 1995/01/01/ 1995, doi: https://doi.org/10.1016/0008-6223(95)00092-R.

[71] A. A. Dubale, W.-N. Su, A. G. Tamirat, C.-J. Pan, B. A. Aragaw, H.-M. Chen, C.-H. Chen, and B.-J. Hwang, "The synergetic effect of graphene on Cu2O nanowire arrays as a highly efficient hydrogen evolution photocathode in water splitting," *Journal of Materials Chemistry A*, 10.1039/C4TA03464C vol. 2, no. 43, pp. 18383-18397, 2014, doi: 10.1039/C4TA03464C.

Appendix A- Setup of the installation and results

A.1 Preparation of the CMSMs

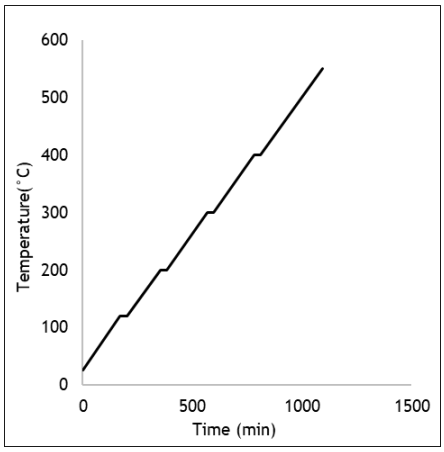


Figure A.1. Carbonization steps to prepare the cellulose-based CMSMs.

A.2 Installations of the different separation tests

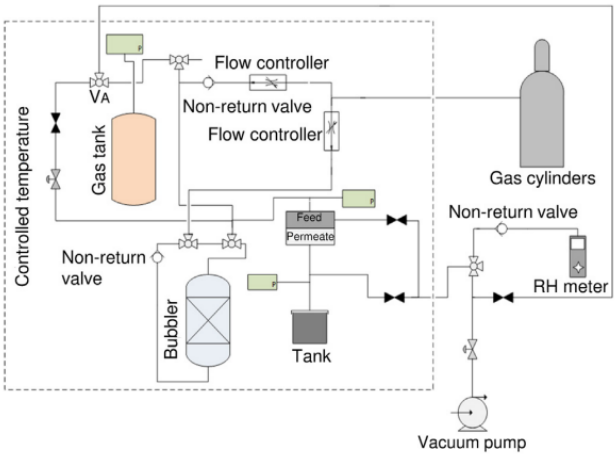


Figure A.2. Experimental setup for single gas permeation experiments (reproduced from [11]).

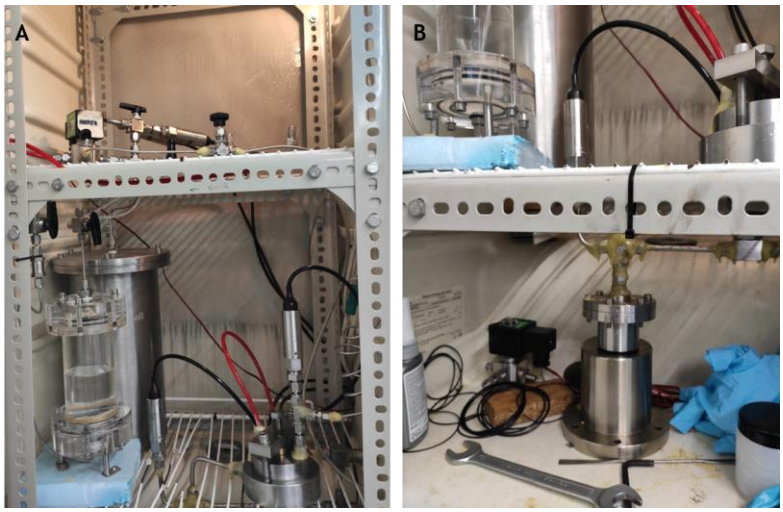


Figure A.3. Photographs of the laboratory installation for single gas permeation tests; (**A**) feed to the membrane module and (**B**) permeate tank.

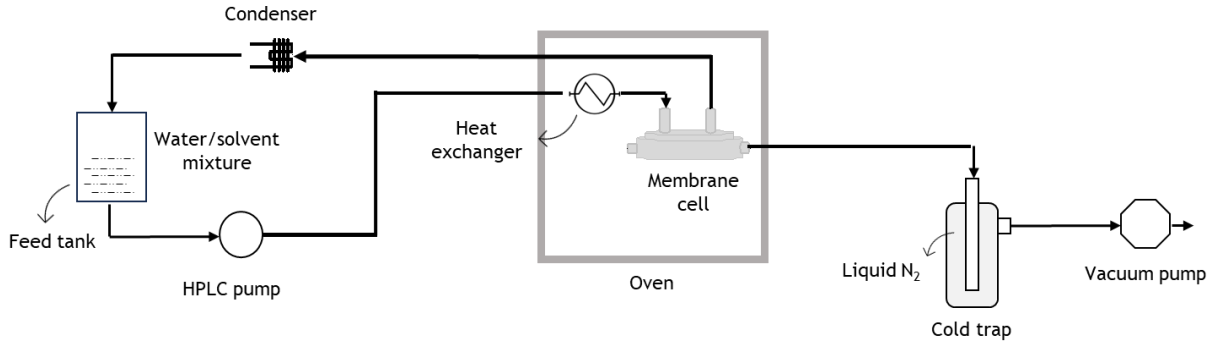


Figure A.4. Initial installation for water/solvent separation tests.

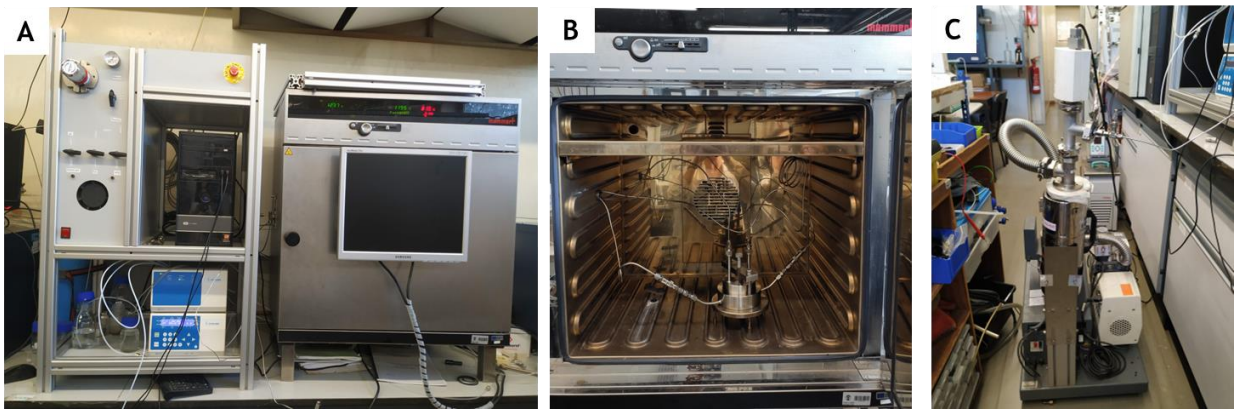


Figure A.5. (**A**) Photographs of the initial laboratory installation for water/solvent separation tests and a (**B**) close up of the membrane module inside the oven and (**C**) the cold trap with a vacuum pump.

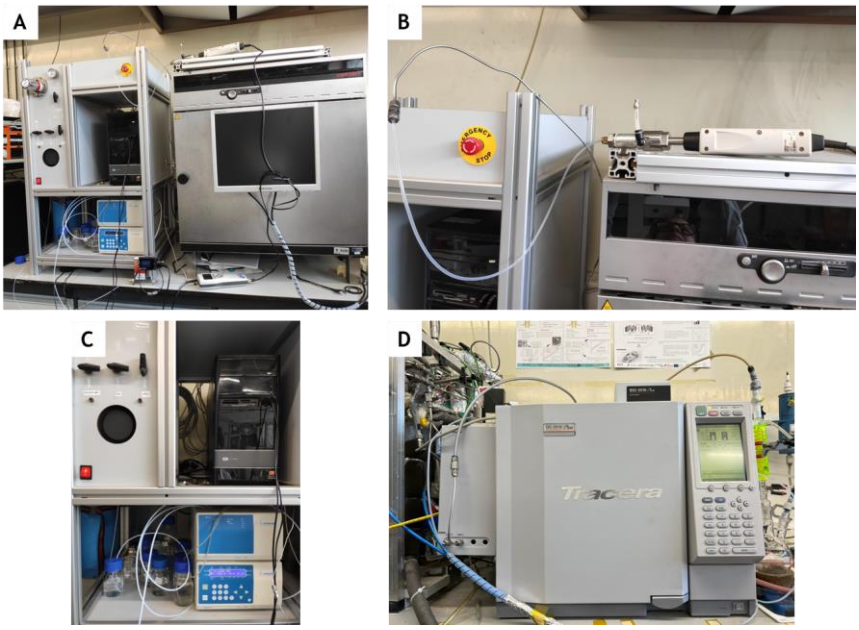


Figure A.6. Photographs of (**A**)the laboratory installation for water/solvent separation tests using the dew point meter; (**B**) close up of the humidity sensor; (**C**) close up of the feed and HPLC pump and (**D**) close up of the GC.

A.3 Deduction of the permeance of the CMSMs to water/solvent permeation tests

The permeate side of the membrane cell can be represented as shown in **Figure A.7**.

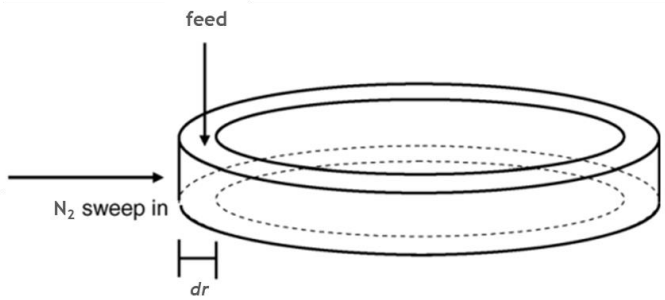


Figure A.7. Flow behavior at the permeate side of the membrane (adapted from [67])

Doing a mass balance over a small part of the permeate side with a thickness *dr*:

$$Q_{H_2O,perm} + Q_{H_2O,perm}\big|_r = Q_{H_2O,perm}\big|_{r+dr} \quad (13)$$

where $Q_{H_2O,perm}$ is the water flow in the permeate. This can be expressed in other form, including the water fraction in the permeate, y_{H_2O} , and the flow rate of the sweep gas, $\emptyset_{N_2}$.

$$\frac{A\ P\ (p_{H_2O,feed} - p_{H_2O,perm})}{l} + y_{H_2O}\ \cdot \emptyset_{N_2}\big|_r = y_{H_2O}\ \cdot \emptyset_{N_2}\big|_{r+dr} \tag{14}$$

where $\frac{P}{l}$ is the permeance, A is the area of the cell and $p_{H_2O,feed}$ and $p_{H_2O,perm}$ are the water vapor pressure on the feed and permeate side of the membrane, respectively. The fraction of water in the permeate stream can be written as $\frac{p_{H_2O,perm}}{P_{total}}$ where P_{total} is the total pressure at the permeate. If r is the radius of the membrane and dr the thickness, then:

$$\frac{2\pi r\ dr\ \ P\ (p_{H_2O,feed} - p_{H_2O,perm})}{l} = \frac{p_{H_2O,perm}}{P_{total}} \cdot \emptyset_{N_2}\Big|_{r+dr} - \frac{p_{H_2O,perm}}{P_{total}} \cdot \emptyset_{N_2}\Big|_{r} \tag{15}$$

This results in:

$$\frac{\frac{p_{H_2O,perm}}{P_{total}} \cdot \emptyset_{N_2}\Big|_{r+dr} - \frac{p_{H_2O,perm}}{P_{total}} \cdot \emptyset_{N_2}\Big|_{r}}{r\ dr} = -\ \frac{2\pi\ P\ (p_{H_2O,feed} - p_{H_2O,perm})}{l} \tag{16}$$

$$\lim_{r\to 0}\left(\frac{\frac{p_{H_2O,perm}}{P_{total}} \cdot \emptyset_{N_2}\Big|_{r+dr} - \frac{p_{H_2O,perm}}{P_{total}} \cdot \emptyset_{N_2}\Big|_{r}}{r\ dr}\right) = -\ \frac{2\pi P\ (p_{H_2O,feed} - p_{H_2O,perm})}{l} \tag{17}$$

$$\frac{d_{p_{H_2O,perm}}}{(p_{H_2O,feed} - p_{H_2O,perm})} = -\frac{2\pi P\ P_{total}\ r}{l\ \emptyset_{N_2}} dr \tag{18}$$

$$\int_{p_{H_2O,perm}}^{0} \frac{d_{p_{H_2O,perm}}}{(p_{H_2O,feed} - p_{H_2O,perm})} = -\int_{0}^{r} \frac{2\pi P\ P_{total}\ r}{l\ \emptyset_{N_2}} dr \tag{19}$$

where the water vapor concentration when the radius is the same as the radius of the cell is zero and the $p_{H_2O,perm}$ is determined when the radius is zero with the dew point meter. The integration results in Equation 11.

Table A.1. Specific constants used in Antoine equation.

A	B	C
5.11564	1687.537	230.17

A.4 Results

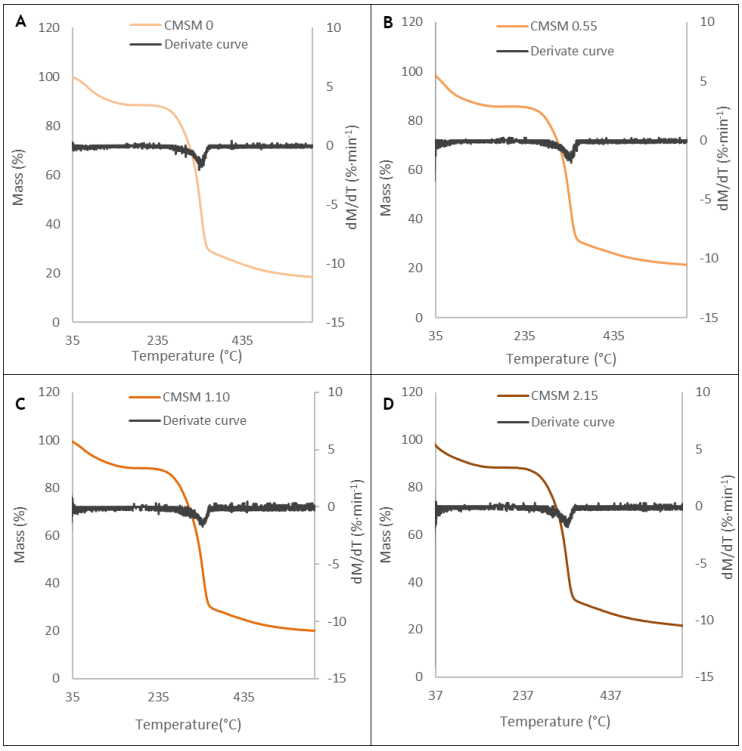


Figure A.8. TGA plot and correspondent derivate curve of the precursor correspondent to (**A**) CMSM 0; (**B**) CMSM 0.55; (**C**) CMSM 1.10 and (**D**) CMSM 2.15.

Table A.2. FTIR spectra bands assignments.

Wavenumber (cm^{-1})	Functional group	Assignment
3,350; 3,623	-OH	-OH stretching
3,024	=CH	=CH stretching
2,898;3,033	$-CH_2$ or CH_3	Aliphatic groups
2,123	-N≡C	N≡C stretching
2,001	Substituted benzene rings	Several bands from overtones and combinations
1,643; 1,573	C=C, C=N, NH	C=C and C=N stretching, NH deformation
1,837	-C=O	-C=O stretching
1,317; 1,473	$-CH_2$ or $-CH_3$	$-CH_2$ or $-CH_3$ bending
1,159;1,143; 894	-C-O-C	-C-O-C stretching
1,012	-C-OH	-C-O stretching
862; 788	Benzene	Aromatic rings

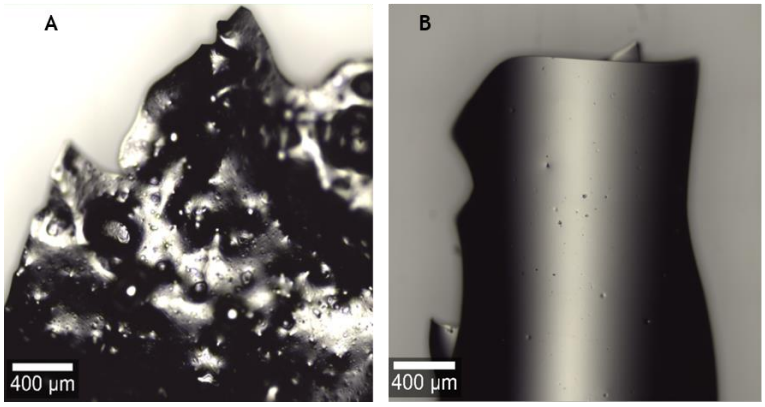


Figure A.9. CMSM surface of a sample (**A**)with and (**B**) without boehmite.

Table A.3. Permeability results for each CMSM tested.

	Permeability (barrer)			
	H_2	CO_2	O_2	N_2
CMSM 0	256	164	35	6
CMSM 0.55	321	146	40	45
CMSM 1.10	567	218	161	5
CMSM CO_2	567	218	161	5
CMSM N_2	274	146	43.6	3
CMSM N_2+H_2	495	256	99	16

Table A.4. Ideal selectivity results.

	Selectivity			
	H_2/CO_2	H_2/N_2	CO_2/N_2	O_2/N_2
CMSM 0	2	43	27	6
CMSM 0.55	2	71	32	9
CMSM 1.10	3	107	41	30
CMSM CO_2	3	107	41	30
CMSM N_2	2	83	44	13
CMSM N_2+H_2	2	30	16	6

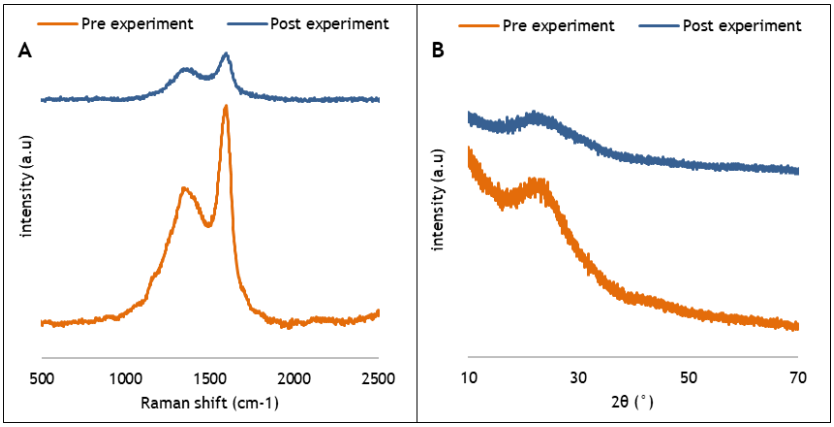


Figure A.10. (**A**) Raman and (**B**) XRD spectra for the CMSM 1.10 pre and post experiment.